Sapienza University of Rome

ARCHMAT

(Erasmus Mundus Master in Archaeological Materials Science)

Scienzee Technologie per la Conservazione dei Beni Culturali

The process of MA-XRF data for spectroscopy imaging in cultural heritage

Laureando: **Fakhriyya Huseynli**

Matricola: **1905618**

Relatore: **Stefano Ridolfi**

Sapienza University

Rome, December 2020

To our 2783 martyrs who lost their lives during II Karabakh war

To my lovely late grandmother-Narin Muradova

I am so sorry that I could not be with you in your last breath

Thanks for everything I miss you

Acknowledgements

Firstly, to God and his guidance during hardest times in my life. Then, the author is wholeheartedly grateful to Education, Audiovisual, and Culture Executive Agency (EACEA) of the European Commission, as well as with the Erasmus Mundus Consortium for her selection and funding to participate in this master programme.

At the same time, I am thankful to the Ars Mensuare Laboratory availability of the equipment needed for the execution of this research and provide me with sample which was painting from private collection. My deepest gratitude is expressed to Professor Stefano Ridolfi for his guidance and supervision during the research. Also I am so thankful to Silvia Scardina, Sergio Lins, Mahir Hrnjic who willingly guided me and inspired me through their passion on science, programming.

I thank Professor Nicola Schiavon as the coordinator of the consortium of ARCHMAT for giving chance be part of this program, coordinator in Aristotle University of Thessaloniki Professor Evangelia Varella, coordinator in University of Rome Sapienza, Professor Donatella Magri, and all of the professors in three universities who taught and shared many knowledges and experiences during the my studies in Europe.

My sincere gratitude for my family who let me to get a higher education, to my father who did not prevent my way to go behind of my dreams. Specially, I am thankful to my brother who inspired, motivated me to continue my education abroad to apply scholarships. However, all ups and downs in my life he is always there for me, without him it would be impossible. Finally, I express my deepest gratitude to best friends Namrin Alakbarli, Susan Yunusova, Shatilla Algaff, Shradda Khalid, Islam Shaheen, Nagm Eldeen my classmates and Shaqquliler. for the emotional and physical support throughout this journey.

Abstract

Scanning macro-X-ray fluorescence analysis (MA-XRF) is rapidly being established as a technique for the investigation of historical paintings. The elemental distribution images acquired by this method allow the visualization of hidden paint layers and thus, provide insight into the artist's creative process and the painting's conservation history.

As a non-destructive instrument MA-XRF and analyzing software PyMca will be used to identify, also to study painting from private collection in Italy. The use of MA-XRF to tentatively predict pigments has an important advantage, its application provides the undamaged and low cost survey of large areas in the painting. The method was proved powerful and useful, capable of efficiently determining the composition and structure of the investigated object in a total safe approach. Nevertheless, for a more throughout evaluation and a better estimation of the pigment composition, it has been demonstrated that, the use of complementary analytical techniques is required.

Keywords: XRF, PyMca, painting, synchrotron radiation, MA-XRF

Abbreviations

1. BSQ-Band-sequential
2. CCD-Charge-coupled device
3. CMOS-complementary metal-oxide semiconductor
4. CU- Control Unit
5. DSP-Digital signal processor
6. DXP- Digital X-ray Processor
7. EDXRF -Energy dispersive x-ray fluorescence
8. FET-Field effect transistor
9. FP- Fundamental Parameters
10. FWHM- Full-Width-at-Half-Maximum
11. HPGe-High-purity germanium
12. HSI-Hyperspectral imaging
13. IFD-Input focal distance
14. INGaAs-Indium Gallium Arsenide
15. IRR- Infrared reflectography
16. IRT-Infrared thermography
17. LEDs-Light-emitting diodes
18. LOD- Limits of Detection cps counts per second
19. MCA- Multi channel analyzer
20. MCT- Mercury Cadmium Telluride
21. MSI-Multispectral imaging
22. MWIR-Mid infrared
23. NAAR- Neutron Activation Auto-Radiography
24. NIR-Near-infrared region
25. NLLS-Non-linear least-squares method
26. OFD-Output focal distance
27. PyMca -Python Multi-channel analyzer
28. RF- Radio frequency
29. ROI- Region of Interest RGB Red-Green-Blue
30. RTOS- Real Time Operative System
31. SDD -Silicon Drift Detectors
32. Si(Li)-Lithium drifted silicon

33. SR- Synchrotron Radiation
34. SWIR-Short-wave infrared
35. The FET -The field effect transistor
36. THL-Tungsten halogen lamps
37. UVF-Ultraviolet-induced fluorescence
38. UV-Ultraviolet
39. VIS-Visible
40. VNIR-Visible -near-infrared
41. WDXRF-Wavelength x-ray fluorescence
42. XOS-X-ray optical systems
43. XRF-X-ray fluorescence
44. XRR-X-ray radiography

TABLE OF CONTENTS

Chapter 1. Introduction 1
Chapter 2. Spectroscopy techniques for cultural heritage 5
2.1. Multispectral and hyperspectral imaging 5
2.1.1 Wavelength selection 10
2.2 Spectroscopy imaging techniques are commonly used in cultural heritage 12
Chapter 3. XRF and MA-XRF 18
3.1 Fundamentals of XRF 18
3.1.1 What are X-rays? 18
3.1.2 Interaction of X-rays with matter 19
3.1.3 X-ray sources 22
3.2 XRF detectors 24
3.2.1 X-ray detectors and multi channel analyzers 24
3.2.2 XRF spectrometer 28
3.2.3 Introduction to MA-XRF 30
3.2.4 Working principles of MA-XRF 31
Chapter 4. Acquisition operation system of MA-XRF 33
4.1 Translation stage and scanning head 33
4.1.1 X-ray optics 35
4.2 DETECTOR 38
4.2.1 Detector efficiency 38
4.2.2 Energy Resolution 40
Chapter 5. PyMca data processing and data collecting 46
5.1 Spectrum analysis 46
5.1.1 Spectra evaluation 46
5.1.2 Peak shape model 47
5.2 PyMca data collecting 49
Chapter 6. Results and discussion 52
6.1 The structure of easel paintings 52
6.2. Elemental distribution images 58
Chapter 7. Conclusion 62
Bibliography 64

List of figures

Figure 1. X-rays and other electromagnetic radiation 19
Figure 2. Three main interaction of X-ray matter (photo by PANalytical) 19
Figure 3. Appearance of Rayleigh and Compton peaks in XRF spectrum (photo by PANanlytical) 20
Figure 4. Principial allowed transitions producing X-ray characteristic emissions 21
Figure 5. Design of X-ray tube (photo by PANanlytical) 23
Figure 6. Graphic scheme of a gas-filled detector (photo by PANanlytical) 25
Figure 7. Basic design of a scintillation detector (photoby PANanlytical) 26
Figure 8. Basic design of a solid-state detector (photo by PANalytical) 27
Figure 9. General structure of spectrometer 28
Figure 10. Bruker M6 Jetstream set-up and details of the measuring head 34
Figure 11. Focusing X-ray Optic (photo by XOS website) 37
Figure 12. Collimating X-ray Optics (photo by XOS website) 38
Figure 13. Cutaway diagram showing construction of a large SDD detector 44
Figure 14. Cutaway diagram showing construction of a large SDD detector 44
Figure 15. XRF spectrum fast fitting performed using PyMca software of analyzed painting 46
Figure 16. Analysis software in running on a laptop connected to Control Unit 50
Figure 17. Schematic stratigraphy of an easel painting 53
Figure 18. "Il contadino" 19th century oil on canvas under normal light 55
Figure 19. RGB composite image of the interest area of painting subdivided three areas 55
Figure 20. MA-XRF instrument on "Il contadino" painting (photo by Stefano Ridolfi) 56
Figure 21. ROI image under normal light and grayscale mode 57
Figure 22. XRF spectrum fast fitting with interested elements 57
Figure 23. Zn elemental distribution map under grayscale and colorful scale 58
Figure 24. Cr distribution image under grayscale and colorful scale 59
Figure 25. Fe,Mn,Ba,Ca and Pb elemental distribution map 60
Figure 26. Merge of elemental distribution map under RGB mode 61

Chapter 1. Introduction

In early UNESCO recommendations, Cultural Heritage has been described as "the product and witness of the different traditions and spiritual achievements of the past thus is an essential element in the personality of the peoples of the world". Cultural heritage therefore signifies value, and intuitively gives rise to notions of significance, reflected both in tangible and intangible manifestations of a culture (Forrest, Craig, 2010).

Preserving and interpreting material cultural heritage requires increasingly sophisticated understandings of chemical composition, environmental history, and deterioration mechanisms. Knowledge and understanding of historic materials has conventionally required the removal of samples from objects which are then subjected to analytical techniques. This sampling means that, the process of scientific analysis of artifacts frequently alters or destroys the specimen. Even sub-millimetre sampling "damage" to works of substantial value can be unacceptable for highly valued objects. Particularly, in art examination it is highly desirable that materials be identified without sampling, and without change to the material being studied (Thurrowgood, David, et al.,2016).

Historical paintings can be considered a central part of humanity's cultural heritage; they allow expressing complex messages, allegories and emotions. As they are easily reproducible they can be made available to large audiences. However, the first version of a painting created by the original artist is in general the most apprised (and highest priced), as it's often assumed to represent his or her vision in its purest form and it may still contain traces of the artist's searching hand. This is present in minor or major corrections done to the painting's concept during its creation, which have been often

overpainted and thus hidden from inspection with the naked eye (Alfeld, M., and L. De Viguerie, 2017).

Pigment identification can be used by conservation scientists to elucidate the artist or workshop source of materials used in a painting, to understand how a painted surface has been altered over time hence informing how an artwork is to be conserved and to identify anachronistic uses of materials that could be associated with either fakes and forgeries or associated with past restorations (Pouyet, Emeline, et al ,2020).

Scientific investigations by spectroscopic imaging methods allow visualizing these changes of concept, provide insight in the studio practice of artists and look over their shoulder during the creation of the artwork. Such investigations also help to distinct between the original version of a painting and later versions by the same artist, resp. studio copies by students, which is not always straightforward based on visual inspection or chemical analysis of a few isolated spots (Alfeld, M., and L. De Viguerie, 2017).

At times scientific investigations allow rediscovering discarded works of artists, which were abandoned and overpainted, in general for economic reasons, and thus hidden under later paintings by the same artist. The identification of the pigments used in a work allows gaining insight in the palette of a specific artist and to determine a probable time window for the creation of an artwork. Finally, the precise determination of the state of an artwork and the indication of previous, often undocumented, restorations support the planning of future conservation treatments to preserve the art works for coming generations.

Given the value and the unique nature of historical paintings it is obvious that their investigation requires minimal or non-destructive investigations and that even direct contact with the surface of a painting should be avoided in order to prevent damage.

This is not withstanding, samples taken from the painting and prepared as cross-section provide uniquely detailed insight in the stratigraphy and present currently the best opportunity to gain insight in chemical processes in the painting (Alfeld, M., and L. De Viguerie, 2017).

The distribution of pigments in a painting is very heterogeneous. Pigments (or other inorganic materials) in different layers all produce secondary X-rays, complicating the interpretation of results. Furthermore, due to the limited number of spots that can be analyzed in a feasible amount of time, only local point information is obtained, which is not necessarily representative of the whole painting (Saverwyns, Steven, Christina Currie, and Eduardo Lamas-Delgado., 2018).

A primary tool for these tasks is macro X-ray fluorescence (MA-XRF), a non-invasive method that has become common place in cultural heritage to examine how elements related to various pigments are distributed across a painted surface (Pouyet, Emeline, et al ,2020).

The MA-XRF technique has gained great prominence, due to the possibility of making images of the elemental distribution of large areas in artworks, including of elements of low atomic number which are hard to detect by conventional methods. The images obtained by the technique bring a series of information which allows one to investigate pigments applied, including those just below the visible painted layer of a painting, thus revealing hidden information such as modifications made by the artist himself, overlapping pigments, and surface restorations.

Currently, there are portable MA-XRF instruments with lateral resolution below 100μm, which allow *in situ* analyses of artworks. The history of the evolution of the MA-XRF technique goes through experiments carried out in synchrotron sources. An advantage of carrying out MA-XRF experiments with synchrotron sources is that it

offers the possibility of carrying out other types of investigations, such as X-ray absorption measurements for elemental speciation, even simultaneously. Another advantage is the possibility of reaching small beam spots, which produce high resolution maps, without losing elemental sensitivity, due to the high brilliance of synchrotron light sources. (Pereira, Marcelo & Felix, Valter & Oliveira, Ana & Ferreira, Douglas & Pimenta, André & Carvalho, Cristiano & Silva, Fabricio & Pérez, Carlos & Galante, Douglas & Freitas, Renato., 2020). Results can be plotted as elemental distribution maps. These images can make interpretation more straightforward and since the points analyzed cover a wide surface area, they are more representative of the whole painting. Moreover, discussing images instead of raw spectra with conservators, art-historians and other non-XRF experts is infinitely more conducive to useful exchanges during multidisciplinary projects (Saverwyns, Steven, Christina Currie, and Eduardo Lamas-Delgado., 2018).

In this work, the combined use of PyMca software and MA-XRF analysis has been put to use in an attempt to attest the authenticity of 19th century painting from XX century Italian private collection which was named as “Il contadino”.

Chapter 2. Spectroscopy techniques for cultural heritage

2.1. Multispectral and hyperspectral imaging

Human vision is only able to see in a restricted part of electromagnetic spectrum and can distinguish objects based on their different spectral responses in that narrow spectral range (Khan, Muhammad Jaleed, et al. 2018). However, multispectral imaging sensors have been developed that are able to acquire an image in infrared and visible segments of electromagnetic spectrum. This allows material identification on the basis of their unique spectral signature in a wide spectral range (Khan, Muhammad Jaleed, et al, 2018).

Multispectral and hyperspectral techniques extend the measurable spectrum from visible light to UV (10 nm+380 nm) and IR (750 nm+1 mm) lights with increased resolution: typically multispectral imagery has three to ten bands, while hyperspectral imagery could have hundreds or even thousands of narrower (e.g., 10 nm) bands (Huang, Xiang, et al. 2016).

Multispectral imaging exploits the property that each material has its own unique spectral signatures. Spectrum of a single pixel in a multispectral image provides information about its constituents and surface of the material. Multispectral imaging technology is being used for environment and land observation remote sensing in satellite and airborne systems since late 1960s. These systems acquire data in a small number of spectral bands by using parallel sensor arrays (Khan, Muhammad Jaleed, et al. 2018). MSI and HSI can be regarded as common technology for the field of restoration and conservation of artworks (Klein, Marvin E., et al. 2008).

However, spectroscopy only produces a mean spectrum-based average measurement of a sample, irrespective of the whole area of the sample being analyzed. As the spectra collected are averaged to provide a single spectrum, the information on spatial distribution of constituents within the sample is thus lost. That is why spectroscopic

techniques cannot be considered comprehensive inspection tools, especially for heterogeneous samples, due to their lack of spatial information. Thus, hyperspectral imaging (HSI) has been introduced. The term "hyperspectral imaging" was first used by Goetz (1985) for remote sensing to make a direct identification of surface materials in the form of images (Khan, Muhammad Jaleed, et al. 2018).

Hyperspectral imaging (HSI), studies how the light interacts with the observed materials, measuring the amount of light that is emitted, reflected or transmitted from a certain object or target. HSI sensors usually operate in the 0.4 to 2.5μm spectral region, capturing the visible and solar-reflected infrared spectrum (i.e., the near-infrared or NIR, and the short-wavelength infrared or SWIR) from the observed materials (Paoletti, ME, et al. 2019).

Hyperspectral image is a 3D data cube, which contains two-dimensional spatial information (image feature) and one-dimensional spectral information (spectral bands). Especially, the spectral bands occupy very fine wavelengths, while the image features such as land cover features and shape features disclose the disparity and association among adjacent pixels from different directions at a confident wavelength (Gogineni, Rajesh, and Ashvini Chaturvedi. 2019).

During the last three decades, multi-spectral and hyperspectral imaging technology, implemented on satellite and aero plane-based platforms, has found an enormous range of applications in many subjects, such as mineralogical mapping of the earth's surface, agricultural and environment control, and military defense. Spectral imaging techniques have also found a wide spread use in microscopic analysis of biological targets for the identification and mapping of skin tumors , and the study of plant, animal and human tissues for various purposes. In the field of conservation of artistic and historic objects, such as paintings and documents,

multispectral and hyperspectral imaging has a long tradition as a non-destructive tool for the surveying of underdrawings, additional touches and, to a certain degree, pigments identification (Padoan, R., et al. 2008).

A spectral imaging system needs the following essential components: radiation source/lighting, focusing optics, detector and wavelength selection the most important thing. There is a diverse range of methods for wavelength selection which determines the design of the illumination system and the spatial and spectral scanning strategy (Liang, Haida, 2012).

HSI systems can be classified in many different ways based on image acquisition mode (whiskbroom, staring, or push broom), spectral ranges (UV, Vis, NIR, MIR), or measurement mode (reflectance, transmittance, or interactance). However, the fundamental classification scheme of HSI systems is based on the acquisition mode, how spectral and spatial information is acquired. The conventional HSI system involves two scanning methods: spatial scanning (point scanning and line scanning) and spectral scanning (area scanning). Therefore the three approaches for generating a hypercube are point, line, and area scanning. In point scanning (also known as whisk-broom imaging), a spectrum is acquired at a single spatial location, and then other points are scanned by moving either the detector or the sample. This procedure is repeated for each spatial position at which spectral data is required. The advantage of a whisk-broom scanner is that the light passes through the same path in the optical system for each spatial point measurement. This technique is commonly used for Raman HSI and is typically the most time-consuming way to obtain HSI data. Line scanning (also known as push-broom imaging) records spectral information simultaneously. This is done line by line and requires relative movement between the sample and detector. It is usually 100 times faster than point scanning and is convenient to implement in conveyor belt systems. Spectral scanning approaches usually store hypercube in band-

sequential format (BSQ), which compromises performance between spatial and spectral information, while spatial scanning stores the hypercube either in the form of band interleaved by pixel (BIP) or band interleaved by line (BIL), both of which perform well in spatial and spectral analysis (Kamruzzaman, M., and DW. Hedgehog. Academic Press, 2016).

The fundamentals of spectral imaging are based primarily on the interaction of light with matter. Light and other electromagnetic radiations are commonly described in terms of their wavelengths, but the designation of spectral ranges varies often with the application, especially for the infrared. To be consistent with the papers described in this review, the following nomenclature will be used – visible (VIS): 0.4–0.7 μm; near-infrared (NIR): 0.7–1.0 μm; short-wave infrared (SWIR): 1.0–2.5 μm; and mid-infrared (MWIR): 2.5–15 μm. The near-infrared range is sometimes grouped with the visible and referred to as visible-near-infrared (VNIR) (Liang, Haida, 2012).

There are three common measurement modes for hyperspectral imaging, namely reflectance, transmittance or interactance. They differ in lighting and detector configurations, resulting indifferent effects on data acquisition for the same substance. The appropriate acquisition mode depends on the type of sample and the constituent or property being analyzed. Reflectance mode is easy to use without any contact with the substance, and light level is reasonably high relative to the sample. Reflectance mode can obtain high relative information from the sample. In the transmittance mode the amount of light penetrated through the substance is often very small but carries more valuable information and the detector is located on the opposite side of the light source to capture the transmitted light through the sample. The interactance mode is a combination of the reflectance and transmittance modes. In the interactance mode, the light source and the detector are on the same side of the sample; thus this mode has a practical advantage over the transmittance mode, although it needs a light seal to

prevent specular reflection from directly entering the detector. A majority of the HSI systems in the literature were implemented on the reflectance mode. Hyperspectral reflectance imaging detects external quality characteristics such as color, size, shape, and surface defects but is less effective in evaluating internal quality characteristics. The transmittance mode is effective in detecting internal defects and concentrations of transparent materials such as fish, fruit, and vegetables, while the interactance mode measures turbid liquids or semisolids and solids. Reflectance mode can be applied in the spectral range of 400-2500 nm, while the application of transmittance mode is more specific in the wavelength range of 700-900nm or 800-1100nm (Kamruzzaman, M., and DW. Hedgehog. Academic Press, 2016).

Generally, a light source for hyperspectral imaging systems can be classified into two categories: illumination and excitation sources. Broadband lights are generally used as the illumination sources, while narrowband lights are commonly used as the excitation sources. Tungsten halogen lamps (THL) are durable, stable, and generate a smooth spectrum in the visible to infrared wavelength range and are low cost (Kamruzzaman, M., and DW. Hedgehog, 2016).

However, THL generates a significant amount of heat, which could alter the physical and chemical structure of the samples. It is the most common illumination source that has been intensively used in various applications of hyperspectral reflectance and transmittance imaging. Besides a halogen source, broadband light-emitting diodes (LEDs) are also finding applications in hyperspectral imaging systems because of their long life-time, low power consumption, low heat generation, small size, fast response, robustness, and insensitivity to vibration. LED can also cover a wide spectral range, from the visible to the near-infrared region (NIR). However, LEDs covering the NIR range are currently more expensive than tungsten halogen lamps, and LEDs only provide narrow wavebands of light, making them more suitable for multispectral

imaging. Based on the development of new materials and electronics, LED technology is still ongoing and will become a mainstream light source (Kamruzzaman, M., and DW. Hedgehog, 2016).A variety of lasers have been used in hyperspectral fluorescence and Raman imaging. Besides lasers, other types of sources, such as low-pressure metal vapor lamps (eg, mercury), ultraviolet (UV) fluorescent lamps, and high-pressure arc lamps (eg, xenon), are also competent for the demands of excitation sources (Kamruzzaman, M., and DW. Hedgehog, 2016).

One of the special requirements for imaging of heritage objects is minimum light exposure to ensure that light-induced ageing of the objects is kept at a minimum. There is a vast body of work done on light-induced ageing which has in-formed display strategies in museums. In general, UV and thermal radiation are eliminated from a white light source before it is used to illuminate objects in museums. For example, for oil paintings the recommended levelis~200 lux and for manuscripts and other paper-based art-works the lighting level is kept at~50 lux. It is generally assumed that the reciprocity principle holds, which basically says that light-induced damage is determined by the accumulated total energy incident on a material rather than the intensity of the incident light. The reciprocity principle has been widely used to justify high intensity illumination for fast imaging. To achieve the same signal-to-noise ratio in an image, one can either illuminate the object with a low intensity light for longer or a high intensity light for a shorter period of time. Since it is the total energy incident on an object that determines the damage, it appears sensible to use a higher intensity light to increase the imaging efficiency without causing extra damage (Liang, Haida, 2012).

2.1.1 Wavelength selection

Wavelength selection can be achieved either on the illumination light path such that only a selected wavelength range of light is incident on the object at a time, or on the

reflected light path before the detector such that the light reflected from the object can be separated spectrally.

Wavelength selection through illumination

The first multispectral imaging system designed for paintings was through filtering the illumination and using a monochrome digital camera to collect the reflected light. Interference filters were placed in front of a halogen-tungsten light source. The advantage of such a system is economic light exposure since only a narrow wavelength range is incident on the object at a time. The other advantage is that any off-the-shelf monochrome camera and lens system can be used without modification.

Wavelength selection in the reflected light

Alternatively, wavelength selection can be achieved through either filtering or dispersing the reflected light. In the snapshot mode, the entire spectrum is collected simultaneously per spatial point and a spatial area is collected through scanning in a time sequence. In the sequential mode, the spatial field of view is imaged through one wavelength channel simultaneously and the full spectral cube is collected through sequential spectral filtering. The snapshot mode has its advantage when imaging objects that are time varying over a time scale shorter than the imaging time (Liang, Haida, 2012).

The performance of the detector directly determines the quality of the images. Generally, a high sensitive detector with high signal-to-noise ratio is required. A charge-coupled device (CCD) and complementary metal-oxide semiconductor (CMOS) are the two widely used detectors that have been rapidly developed. Both types of detectors are sensitive in the visible and short wavelength near-infrared regions (400-1000 nm). They cannot be used for long-wave NIR applications as Si CCD detectors

need coating, which reduces the quantum efficiency in long-wave applications. Some specific advantages of CMOS detectors include low cost, low power consumption, single power supply, and small size for system integration, which makes them competitive in the consumer electronics market (Kamruzzaman, M., and DW. Hedgehog, 2016).

For low noise detection, Peltier cooled systems are preferred. In the Short Wave Infrared(SWIR) range between 900 nm–1700 nm and wider wavelength region (900-2500 nm), mechanically cooled Indium Gallium Arsenide (In GaAs) or Mercury Cadmium Telluride (MCT) detectors arrays are the commonly use due to their high sensitivity but they are more expensive. While extended InGaAs can reach beyond 2 μm, they cannot compete with HgCdTe in sensitivity. HgCdTe detectors are sensitive to abroad wavelength range from~1μmto~10 μm. Currently, spectral imaging have mostly been conducted in the range between 400 nm and 1700 nm, mainly because of the huge jump in cost for detector arrays that are sensitive beyond 1.7 μm. Some early works have pushed this up to 2.2 μm using low sensitivity analogue detectors such as the PbO-PbSvidicon. The only recent device used in art applications that managed to reach 2.3 μm is the one that uses single element InGaAs detectors (Liang, Haida, 2012).

2.2 Spectroscopy imaging techniques are commonly used in cultural heritage

Spectroscopy is the study of the interaction between electromagnetic radiation (or particle) and matter. Spectrometry is the experimental measurement of these interactions. The instrument that performs such measurements is a spectrometer and experimental data concerning the interaction is referred to as a spectrogram or a spectrum. The theory and practice of spectroscopy require a substantial knowledge of the physical properties of the probe, of the mechanisms of the radiation comprising the matter (Artioli, Gilberto, and Ivana Angelini, 2010).

When dealing with paintings, drawings, or other quasi-two dimensional (2D) art objects, imaging techniques are the preferred choice, not only for a preliminary evaluation of the conservation state of the artwork, but also for gaining knowledge on pigments and their distribution on the surface. Choosing the most suitable technique from the different available options depends on the size of the artwork, its value, the research interests and budget. The well-established traditional methodologies, such as ultraviolet-induced fluorescence (UVF), infrared reflectography (IRR), X-ray radiography (XRR) are presently used together with more advanced techniques that enable the acquisition of multilevel information on pictorial materials, their distribution, and to some extent, also on their layering when suitable data-processing algorithms are used. These advanced imaging techniques include, multi-spectral imaging (MSI), hyper-spectral imaging (HSI), Macro X-Ray Fluorescence (MA-XRF), and Time-Domain Terahertz imaging (THz-TDI), to name a few of the most significant (Picollo, Marcello, et al., 2020).

UV fluorescence describes the emission of visible light observed when an electron of a molecule or atom that has been excited to a higher energy state by UV radiation relaxes to its ground state, emitting a photon with energy associated to the difference between the two states. The emission induced on polychrome artworks depends on many factors: the wavelength and bandwidth of the UV source, the painting materials (pigments, dyes, binders, varnishes) and how all of these materials interact with each other and, additionally, how they have aged. UVF is used for the examination of different kinds of historical and archaeological objects, including photographs and textiles, but it is most widely used for polychrome art. UV fluorescence can indeed be used for a preliminary identification of pigments. However, the varnish does play a major role, since it generally exhibits a strong fluorescence which can overwhelm the actual fluorescence of the pigments. Consequently, UVF documentation aiming at

pigments identification is recommended only when the varnish has been removed from the artwork. UVF photography must always be seen as a supplementary technique for pigment identification, since this method can only provide qualitative information on the UV-induced visible fluorescence of materials. For quantitative studies, the UV fluorescence must instead be documented with fluorescence spectroscopy and colorimetric measurement. Specifically in the case of paintings, UV fluorescence largely comes from the surface of the top paint layer, and it is barely influenced by the underlying layers. Conservators pursue UVF photography to identify and evaluate the integrity of old varnish layers and to localize in paints, which generally lack fluorescence, in contrast with the bright appearance of aged varnishes. When the contrast is intense enough, it is possible to implement an automatic segmentation of the UVF image of a retouched painting. This procedure can quicken the workflow for the estimation of the extent of losses, a necessary step in the preparation of condition reports (Cosentino, Antonino, 2015).

Infrared reflectography (IRR) technique is based on the illumination of the painting with infrareds or only visible light (Infrared Fluorescence- IRF) and by recording the reflected infrared radiation. IR radiation penetrates the surface layers of the painting and the under drawing becomes visible, due to the transparency of some pigments, as such as lead white and titanium white. IRR analysis has provided important information for authentication in paintings based on black carbon sketches drawn on a white gesso ground (calcium sulfate). Due to the IR radiation absorption by black carbon and reflection back from the ground, black carbon under drawing become visible (De Boer, JRJ Van Asperen, 1968).

Radiography is a well-established nondestructive, non-sampling, and noncontact technique commonly used by conservators, scientists, and imaging specialists to look into the hidden or internal structure of cultural objects. A properly exposed radiograph

can provide information that might not be visible to the naked eye, such as under painting, hidden metal pins used to repair sculptures, and supporting armatures. This information can be used to illuminate the manufacturing process, artisanal alteration, or prior conservation treatment of objects and structure. Sometimes this reveals conditions that could require conservation treatment intervention. Many major cultural institutions with X-ray facilities and equipment have made discoveries and revealed crucial information for the cultural objects with this technique. Institutions or individuals with limited or no access to X-ray facilities generally cannot benefit from this investigative technique without taking the objects off-site, often at a high cost associated with the analysis and the insurance requirements associated with artifact transport (Chen, Jiuan Jiuan, Aaron Shugar, and Ashley Jehle, 2019).

In IRR the painting is exposed to an IR radiation source and part of the reflected (i.e.un-absorbed) IR radiation is detected .The method is giving best results with paintings that have a strongly reflecting background (such as chalk or gypsum) with(hidden) carbon black layers/lines on top of it. IRR is of limited use if the background is less reflecting or the painting contains pigments that strongly absorb IR radiation in the upper paint layers (Alfeld, Matthias, et al, 2011).

Terahertz research entered the field of cultural heritage conservation in 1998, when Kochet demonstrated the potential of terahertz imaging as a tool for dendrochronology—the science of dating wooden objects. It is the combination of material characterization, time of flight imaging and the penetration of optically opaque materials that gives rise to applications for subsurface imaging of many culturally significant objects. Moreover, the variety and adaptability of the many electronic, optic, and hybrid terahertz sources allows for versatile approaches to measurements. Resolution can be scaled from tens of micrometers to several millimeters, providing mesoscopic details with the possibility of taking measurements without sample

extraction, *in situ*, and in the field. The more powerful non-destructive forms of radiation for imaging, like x-ray, gamma-ray, proton and neutron, are ionizing and are usually available only through large installations between which coordination with cultural heritage institutions can be challenging, both financially and logistically. Because it is non-ionizing, moderate exposure to terahertz radiation poses significantly less long term risk to the molecular stability of the historical artifact and humans than radiation and portable systems are becoming increasingly available. Therefore, terahertz technology provides a nondestructive, non-invasive, portable and non-ionizing toolset for the inference of the construction and life histories of objects and buildings.

In the last 20 years, the number of terahertz imaging applications has dramatically increased with the development of electrical, optical and hybrid-based terahertz technology. As a result, there is a wide variety of 2D and 3D terahertz imaging techniques that have been applied to both the analysis of cultural heritage objects and materials from which they are manufactured. These techniques can be divided into those based on narrow bandwidth (continuous wave or pulsed) terahertz sources operating in the frequency domain and those based on wide band-width (pulsed) sources operating in the time domain, the value of each technique is strongly dependent on the measurement objective (Jackson, J. Bianca, et al. 2011).

In NAAR (Neutron Activation Autoradiography) the painting is exposed to thermal neutrons and a small fraction of the atoms in the paint is transformed to radioactive isotopes. The radiation emitted by these isotopes during their radioactive decay is recorded either via photo plates or (more recently) via image plates. On the basis of the darkening of the plate and the half-life of the radioactive isotopes, the distribution of different elements in the painting can be derived. While NAAR does allow element imaging of specific elements such as Co and Mn, of which the gamma rays can be

detected without overlap with other elements, it requires considerable technical effort and makes the transport of the painting to a neutron source necessary. The painting also needs to be in contact with the photographic recording medium during a prolonged time while it also retains the induced radioactivity for a period of years (Alfeld, Matthias, et al. 2011).

X-ray, visible and infrared range. The visible light ranges from approx. 400–700 nm. In this publication is distinguished between three ranges of infrared radiation: the near infrared (NIR, 700–1000 nm), the short wave infrared (SWIR, 1000–2500 nm) and the mid-infrared range (MIR) above that. The near infrared is often combined with the visible to the VNIR range (400–1000 nm). This distinction is based on the spectral range common detectors are sensitive to and simplifies the categorization of experiments in this paper (Alfeld, M., and L. De Viguerie. 2017).

Chapter 3. XRF and MA-XRF

3.1 Fundamentals of XRF

3.1.1 What are X-rays?

X-rays were discovered in 1895 by Wilhelm Conrad Röntgen at the University of Würzburg, Bavaria. He noticed that some crystals of barium platinocyanide, near a discharge tube completely enclosed in black paper, became luminescent when the discharge occurred. By examining the shadows cast by the rays. Röntgen traced the origin of the rays to the walls of the discharge tube. For his work with x-rays, Röntgen received the first Nobel Prize in physics, in 1901. It was the first of six to be awarded in the field of x-rays by 1927. The obvious similarities with light led to the crucial tests of established wave optics: polarization, diffraction, reflection, and refraction. With limited experimental facilities, Röntgen and his contemporaries could find no evidence of any of these; hence, the designation ''x'' (unknown) of the rays, generated by the stoppage at anode targets of the cathode rays, identified by Thomson in 1897 as electrons (Van Grieken, Rene, and Andrzej Markowicz, eds. 2001).

X-rays or Röntgen rays are defined as an electromagnetic radiation, between γ-rays and ultraviolet radiation possessing energies between 1 KeV and 100 KeV, being divided into "soft" and "hard" X-rays, according to their energy. Its classification is somewhat artificial and some authors define X-radiation as residing between 0.15 KeV and 102 KeV, overlapping part of the hard-ultraviolet and soft γ-radiation (Lins, Sergio Augusto Barcellos, 2018).

The wavelength of x-rays is inversely proportional to its energy according to

$$E=hc/\lambda \quad (1)$$

E- is energy in KeV and λ I the wavelength in nm. The term hc is the product of Planck's constant and the velocity of light and has using KeV and nm a units constant value c=1.23985(Van Grieken, Rene, and Andrzej Markowicz, eds. 2001).

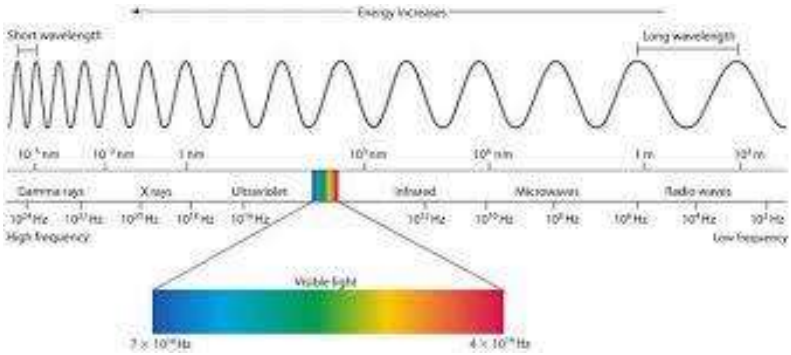

Figure 1. X-rays and other electromagnetic radiation

3.1.2 Interaction of X-rays with matter

Electromagnetic radiation can interact with matter in different levels: rotational, vibrational and electronic. X-radiation, being highly energetic, interacts in an electronic level. There are three main interaction when X-ray contact with matter: fluorescence, Compton scatter and Rayleigh scatter. The fluorescence and the scatter depend on the thickness (d), density (ϱ) and composition of the material on the energy of the X-rays (Brouwer, Peter, 2006). Rayleigh scattering is elastic and refers to the scattering of X-rays caused by atomic electrons in which the energy of the scattered photon remains unchanged.

Compton scattering refers to the inelastic scattering of X-rays, in which part of the incident photon energy is absorbed by an outer shell electron, recoiling and being thus ejected from the atom. The amount of energy of the scattered photon can be easily calculated by the Compton formula (Lins, Sergio Augusto Barcellos, 2018).

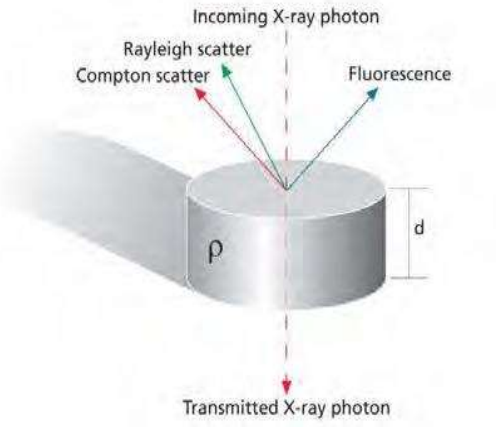

Figure 2. Three main interaction of X-ray matter (photo by PANalytical)

In the process of photoelectric absorption, a photon interacts with an atom in the material. The photon is completely absorbed by the atom and an electron is ejected a vacancy is created in the atomic shell. When this vacancy is filled with an electron from an outer shell, energy is liberated corresponding to the difference in the binding energies of the inner and outer shells (Carlsson, Carl A., and Gudrun Alm Alm Carlsson,1973). The transition can be radiative or nonradiative. If non-radiative, the produced photoelectron will be absorbed by another electron within the atom, generating an Auger electron (or a Coster-Kronig transition, if absorbed by an electron within the same shell). If radiative, a characteristic line is produced in an effect called fluorescence. The probability of obtaining a characteristic line instead of an Auger electron is called fluorescence yield. In other words, the fluorescence yield is the number of emitted X-ray quanta during the filling of the vacancies divided by the number of initial vacancies (Lins, Sergio Augusto Barcellos, 2018). The fluorescence yield increases with increasing binding energy of the photoelectron (Carlsson, Carl A., and Gudrun Alm Alm Carlsson, 1973).

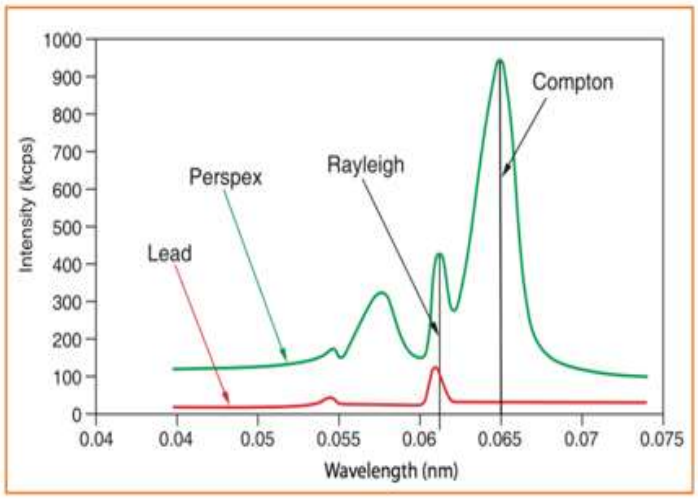

Figure 3. Appearance of Rayleigh and Compton peaks in XRF spectrum (photo by PANanlytical)

The innermost shell is called the K-shell, followed by L-shells, M-shells etc. as one moves outwards. The L-shell has 3 sub-shells called LI, LII and LIII. The M-shell has 5 subshells MI, MII, MIII, MIV and MV. The K-shell can contain 2 electrons, the L-shell 8 and the M-shell 18. The energy of an electron depends on the shell it occupies, and on the element to which it belongs. When irradiating an atom, particles such as X-ray photons and electrons with sufficient energy can expel an electron from the atom (Brouwer, Peter 2006). The K shell electrons, which are the most tightly bound, are the most important for this effect in the energy region considered in X-ray sensitivity (Van Grieken and Markowicz 2002). The energies involved in the transitions are obviously different and will result in detected photons of different energies. If an electron from subshell L2 occupies the vacancy in shell K, the transition is said to be a KL2 transition. If it occurs between subshell L3 and shell K, it is said to be a KL3 transition. KL transitions emit a radiation named Kα, KM transitions produces Kβ radiation. The same is valid for LM and LN transitions, ensuing Lα and Lβ radiations, respectively; and analogously valid for other shell transitions. The subindexes α and β are, in realty composed by the several transition possibilities between the shells (e.g. KL3 and KL2 producing Kα1 and Kα2) as it can be seen in Figure 3. For practical purposes, it is conventional to use the simplified notation referring by Kα the sum of all KL transitions contribution. That being said, the probability of a characteristic X-ray line being produced, for a given sample, can be quantified and is given by a sum of probabilities: the chance of an incident photon, of energy greater than the threshold for removing an electron from an atom, hits the element Z (photoionization cross-section), the probability of a characteristic line within its series (KL2, KL3) is produced and the probability of occurring fluorescence, instead of the production of an Auger electron (fluorescence yield) (Lins, Sergio Augusto Barcellos. 2018).

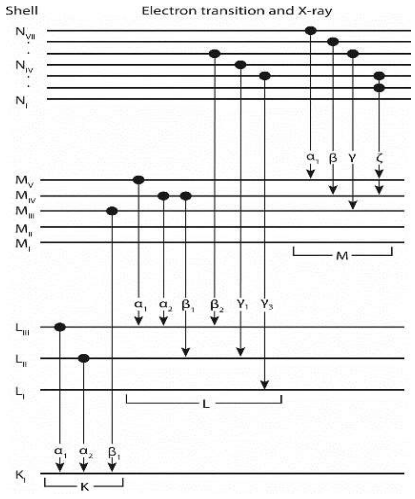

Figure 4. Principial allowed transitions producing X-ray characteristic emissions

3.1.3 X-ray sources

XRF technique is based on the detection of the characteristic fluorescence lines. The fluorescence emission can be induced on a sample through different kinds of sources. In particular, X-rays sources are based on two different principles: the spontaneous radioactive decay of isotopes and the interaction of accelerated electrons with matter (X-ray tubes) or with magnetic fields (accelerators or storage rings).

The use of natural sources shows several advantages, they are: compact, low cost, continuously radiating at high constancy, independent on surrounding conditions and do not need any power supply. The great limitation is their radiation hazard potential, leading to very stringent safety conditions. For this reason the natural sources are unsuitable to be employed in portable instruments.

X-radiation can be generated by any charged particle undergoing centripetal acceleration. Mostly known, is the synchrotron radiation (SR) emitted by electrons or positrons in storage rings that circulate at constant relativistic energies (typically ranging from a few hundreds of MeV to several GeV) or similar circular high-energy particle accelerator facilities. SR is a highly polarized and intense radiation emitted in very short pulses of a few p-s to n-s duration. The radiation is concentrated in a cone tangent to the curved trajectory of the charged particle initiating it, allowing access to several tenths of experiments simultaneously, on the dedicated beamlines (Codling, K., Gudat, W., Koch, E. E., Kotani, A., Lynch, D. W., Rowe, E. M., ... & Toyozawa, Y, 2013). X-ray synchrotron radiation presents some main advantages: high intensity beam of several order of magnitude higher than that reached with X-ray tubes, the monochromaticity of the beam that in some cases can simplify data evaluation, and the advantage to use highly parallel beam, so that it is easier focus and collimate respect to the beam emitted from an X-ray tube. X-ray tubes generate polychromatic radiation with limited intensity; however, the main advantage consists in their portability. XRF analyses have been based on the employment of X-ray tubes as primary radiation.

X-ray tubes (Figure 5.) contain a filament (wire) usually made of W anode (usually made of Mo, Rh, Rd or W) placed in a vacuum housing. An electrical current heats up the filament and electrons are emitted. A high voltage (20-100kV) is applied across the filament and the anode, this high voltage accelerates the electrons towards the anode. When the electrons hit the anode they are decelerated which causes the emission of X-rays. This radiation is called Bremsstrahlung ("Brems" is German for decelerate,

"strahlung" for radiation). The energy and intensity of the emitted X-rays is uniform but spectrum energies are emitted with own intensity.This part of spectrum is often called the continuum because it is a continuous band of emitted energies. A fraction of the electrons that hit the atoms in the anode will expel electrons from these atoms, causing emission of characteristic radiation. The energy of this radiation is determined by the element(s) in the anode (Brouwer, Peter, 2006).

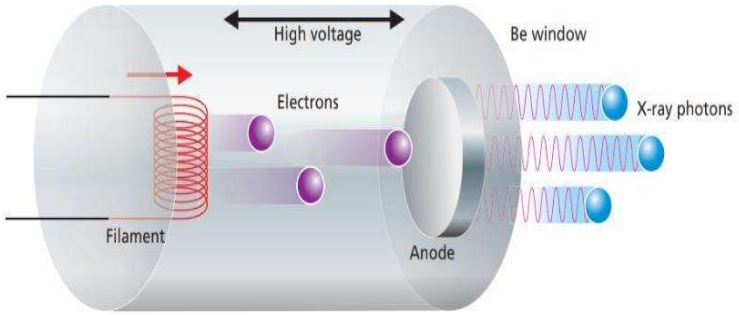

Figure 5. Design of X-ray tube (photo by PANanlytical)

3.2 XRF detectors

3.2.1 X-ray detectors and multi channel analyzers

An X-ray detector is a transducer for converting X-ray photon energy into voltage pulses. The X-ray photon, entering the detector`s active area, interacts through the process of photo-ionization and produces a number of electrons. The current produced by these electrons is converted to digital voltage pulse which corresponds to the energy of X-ray photon (Lifshin, Eric, ed. John Wiley & Sons, 2008). Detectors produce an electrical pulse when an X-ray photon enters the detector, and the height of this pulse is proportional to the energy of the incoming photon. The pulses are amplified and then counted by a multi channel analyzer. There are three important properties of detection systems: resolution, sensitivity and dispersion.

Resolution is the ability of the detector to distinguish between different energy levels. A high resolution means that the detector can distinguish between many different energies.

Sensitivity indicates how efficiently incoming photons are counted. If for instance a detector is very thin, incoming photons may pass it without producing a pulse. Sensitivity is high if the ratio of the number of pulses against the number of incoming photons is high.

Dispersion indicates the ability of the detector to separate X-rays with different energies. A high dispersion means that different energies are separated well.

The Multi channel Analyzer (MCA) counts how many pulses are generated in each height interval. The number of pulses of a certain height gives the intensity of the corresponding energy. The ability of the detector and MCA to distinguish between different energies is called the resolution (Brouwer, Peter 2006).

There are three main types of detector systems in the market which are used in XRF analysis- gas-filled, scintillation detectors and semiconductor detectors. While gas flow proportional counters are ideal for longer wavelengths, they are insensitive to shorter wavelengths. For shorter wavelengths, scintillation counters are employed (Lifshin, Eric, ed. John Wiley & Sons, 2008).

Gas-filled detectors consist of a metal cylindrical tube (often of Al) of about 2cm in diameter, carrying a thin (25-50μm) W wire along its radial axis which is raised to a

high voltage (1300-2000 V). A Be window allows X-ray photons to enter the detector that is filled with an inert counting gas (e.g., Ne,Ar Kr , Xe or He).A schematic of this type of detector is shown below (Margui, Eva, and Rene Van Grieken, 2013).

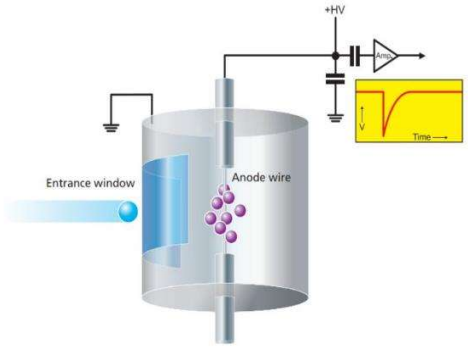

Figure 6. Graphic scheme of a gas-filled detector (photo by PANanlytical)

The operation of a gas-filled detector involves the generation of a small-counts electrons when X-ray photons enter the gas-filled detector. The electrons then reach the anode wire and cause a drop in the voltage which is registered as a negative pulse in the amplifier. The number of electrons is proportional to the energy of the incoming radiation and thus the height of the pulse (Margui, Eva, and Rene Van Grieken. 2013). The main disadvantage of gas detectors is their low density that results in a low efficiency for x-ray detection unless the detectors are made rather large (Kanngießer, B., N.Langhoff, and R.Wedell. *Beckhoff, B., Kanngiesser, B., Langhoff,N.,Wedell,R.,Wolff,H.,Eds*, 2006).

An alternative with much higher detection efficiency for high energy photons is the scintillation detector. Scintillation detector consists of four main parts: a beryllium window, NaI scintillator crystal and a photo multiplier tube with Sb/Cs photo cathode. X-ray photons pass through the beryllium window and hit the scintillator crystal, which producing a blue light flash. The light photons travel into the photomultiplier tube and impact on the photo cathode producing a burst of electrons, which are accelerated through a series of dynodes to the anode. When the resulting electrons reach the anode they cause a drop in voltage. This is registered as a negative voltage pulse in the amplifier. The number of electrons is proportional to the energy of the incoming radiation, and hence the height of the pulse (Brouwer, Peter, 2006).

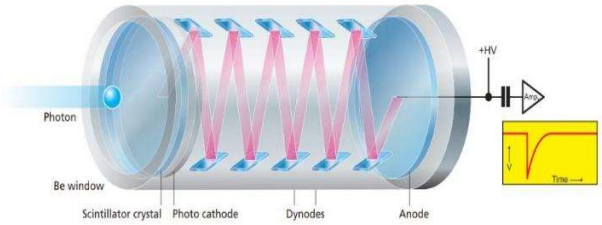

Figure 7. Basic design of a scintillation detector (photoby PANanlytical)

While early observations of ionizing radiation were made by looking at fluorescence screens in darkened laboratories, state-of-the-art scintillation detectors use a scintillating material coupled to photo multipliers, photodiodes or CCDs for the detection of fluorescence light. The benefit of these detectors is that they can be made very small and effective for hard x-rays by using scintillating crystals of heavy elements. Depending on the scintillator, the speed of these detectors can also be increased. When large areas of scintillating material are coupled to a large number of light detectors, a high-efficiency imaging detector is obtained that can be used for, e.g. medical applications. The disadvantage of scintillation detectors is their poor energy resolution (Kanngießer, B., N. Langhoff, and R. Wedell*Beckhoff, B., Kanngiesser, B., Langhoff, N., Wedell, R., Wolff, H., Eds.*, 2006).

Whereas for semiconducting detectors, the material is doped in a manner that electronic "gaps" are created (p-doping) or an enrichment in electrons is made (n-doping), decreasing the conductivity of the material. These offered a much higher resolution than the gas detectors and scintillators. The reason is that the mean energy needed to create one primary elementary charge is about 20–30 eV for gases while for semiconductors it is only a few electron volts. Thus, a ten times higher number of primary charge carrier is produced reducing the statistical fluctuations by about a factor of 3. Furthermore, the higher charge generated allows for the direct measurement by low-noise electronics. (Kanngießer, B., N. Langhoff, and R. Wedell*Beckhoff, B., Kanngiesser, B., Langhoff, N., Wedell, R., Wolff, H., Eds.*, 2006). Semi-conductor detector is constructed with a body of lithium drifted silicon (Si(Li)) or high-purity germanium (HPGe). A beryllium window allows X-ray photons to enter the detector. On the front there is a dead layer and on the back there is a collecting plate. Photons pass through the windows and penetrate produce electron-hole pairs in the body. The number of electrons depends on the energy of the incoming photons. The higher the energy the more electrons will be produced. A high voltage (1500 V) across the dead layer and the back means that the electrons are attracted to the back. When the

electrons reach the back, the potential drops and gives a negative pulse. The depth of the pulse is proportional to the number of electrons and hence proportional to the energy of the incoming radiation. After amplification, a MCA counts the pulses (Brouwer, Peter 2006, Margui, Eva, and Rene Van Grieken, 2013).

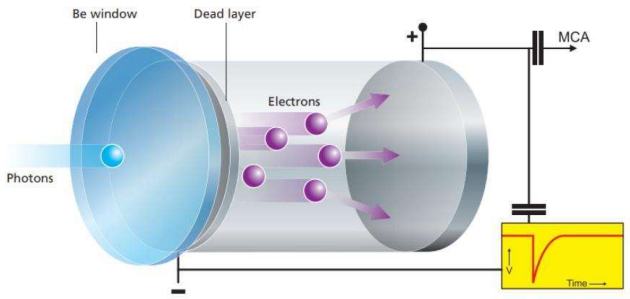

Figure 8. Basic design of a solid-state detector (photo by PANalytical)

One of the main disadvantages of the planar Si(Li) and Ge(Li) detectors is the need for liquid nitrogen cooling. The vacuum-isolated cryostats make these detection systems rather large and difficult to handle. The reason for the cooling the high leakage current at room temperature combined with a rather high read-out capacitance, because these detectors form a plate condenser with the capacitance proportional to the area. The high capacitance results in a high contribution of the serial noise component that requires longer shaping time. For long shaping time, however, the shot-noise contribution from the leakage current increases (Kanngießer, B., N. Langhoff, and R. Wedell*Beckhoff, B., Kanngiesser, B., Langhoff, N., Wedell, R., Wolff,* H., Eds, 2006).

The resolution of gas-filled and scintillation detectors are very poor, and they are not suited for energy dispersive spectrometers. They can however be used in wavelength dispersive spectrometers because, in these instruments, the resolution is achieved by the diffraction crystal. The sensitivity depends on the type of detector and on the energy of the incoming X-rays. Gas-filled detectors have a high sensitivity for low energies and a low sensitivity to high energies and are so best suited to detecting lower energies. The opposite applies for scintillation detectors, which are better suited to high energies than to low energies. Solid-state detectors in general have a very low sensitivity to low energies and high resolution for the higher energies. EDXRF spectrometers commonly

use solid-state detectors, while WDXRF spectrometers use a combination of gas-filled and scintillation detectors (Brouwer, Peter 2006).

3.2.2 XRF spectrometer

X-ray fluorescence (XRF) allows the determination of the elemental composition as well as the quantitative analysis of a wide range of inorganic materials. Results can be expressed as atom percent or weight percent. Often, by custom, especially in the analysis of minerals and rocks, the data are expressed as oxides, stoichiometrically binding the oxygen to the dosed cation (Acquafredda, Pasquale. 2019). X-ray fluorescence (XRF) is a firmly stablished technique, which possesses several fundamental prerequisites for cultural heritage scientists: it can be performed in-situ, it's fast, efficient, safe, non-destructive and can be used to investigate a variety of materials, from glazed ceramics, to paintings and metals, yielding information such as pictorial technique, conservation state, authenticity and manufacturing. Nonetheless, when dealing with inhomogeneous and stratified samples – which is often the case of cultural heritage objects – the results obtained can lead to misleading interpretations (Lins, Sergio Augusto & Gigante, Giovanni & Cesareo, R. & Ridolfi, Stefano, 2019).

The main parts of a spectrometers are source, a sample and detection system (Brouwerw, Peter 2006).

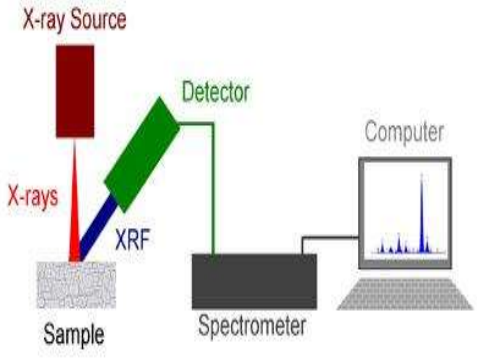

Figure 9. General structure of spectrometer

The basic function of the spectrometer is to separate the polychromic beam of radiation coming from the specimen in order that the intensities of each individual characteristic line can be measured. A spectrometer should provide sufficient resolution of lines to allow such data to be taken, at the same time providing a sufficiently large response above background to make measurements statistically significant, especially at low analyte concentration levels. It is also necessary that the spectrometer allow

measurements over the wavelength range to be covered (Lifshin, Eric, ed. John Wiley & Sons, 2008). X-ray spectrometers may use either the diffracting power of a single crystal to isolate narrow wavelength bands (wavelength dispersive XRF [WDXRF]) or an energy-selective detector to isolate narrow energy bands (energy-dispersive XRF [EDXRF]) from the polychromatic radiation (including characteristic radiation) that is produced in the sample (Liritzis, Ioannis, and Nikolaos Zacharias, 2011).

The classical set-up of WDX uses a crystal that disperses the x-rays and a detector placed at the position where the respective energy is diffracted, counting the photons. In most cases, proportional counters or scintillators are used for this purpose (Kanngießer, B., N. Langhoff, and R. Wedell*Beckhoff, B., Kanngiesser, B., Langhoff, N., Wedell, R., Wolff, H., Eds*, 2006).

In the case of WD analyses (WD-XRF), the technique is normally considered destructive (but rare exceptions), because the sample normally has to be ground and subsequently treated with organic binders or with other components in order to obtain a powdered pellet to submit to analysis. The indisputable advantage remains, compared to the cases of the analyses that require the solubilization of the sample, that the prepared specimen, can be reanalyzed, either with another XRF spectrometer or with other analytical instrumentation, even after many years, provided that it has been well preserved. The amount of sample required for chemical analysis by WD-XRF varies, depending on the kind (qualitative/quantitative) of the searched information and depending on the method and the instrumentation used, from a few tens of milligrams (about 40 mg) up to about 12 g. In some cases, as in provenance determination of obsidians studies, it is possible to use the WD-XRF method also in an absolutely non-destructive way (Acquafredda, Pasquale, 2019).

In the case of ED analyses (ED-XRF), the specimen is normally analyzed as it is and therefore the technique is considered non-destructive. As a matter of fact, the ED counters can provide quantitative or semi-quantitative results even on samples with irregular surface because they suffer much less than the WD techniques from the sample geometry. A wide variety of materials from rocks, to minerals, industrial products, building materials, metals, pigments, etc., can be analyzed by XRF; practically almost everything that is a solid substance and in many cases also liquid or gelatinous substances. Sampling and sample preparation will depend on the used analytical method non-invasive analysis (no sampling) is also possible by XRF and this opens up a

very wide range of applications, especially in the field of Cultural Heritage, where the characterization of precious objects cannot justify their partial destruction (sampling) which would greatly reduce their value (Acquafredda, Pasquale , 2019).

3.2.3 Introduction to MA-XRF

X-ray fluorescence (XRF) is an efficient, fast, safe and firmly established method for the single spot measurement of elements present in paintworks. The generalisation of this technique to a series of points covering a large area, initially developed with Synchrotron XRF , has been transposed to the laboratory in the form of scanning macro XRF (labelled MA-XRF), an imaging technique increasingly used for the investigation of painted artworks (Ravaud, E., et al., 2016).

Scanning macro-XRF (MA-XRF) is a variant of XRF imaging that allows visualization of the distribution of elements in a flat, macroscopic sample (up to several square meters) in a nondestructive manner. This is achieved by scanning the surface of the sample with a focused or collimated X-ray beam of (sub) mm dimensions and analyzing the emitted fluorescence radiation. Due to the penetrative nature of X-rays, elements present at and below the surface contribute to the obtained elemental distribution images. The method is highly valuable in the investigation of historical paintings, as elemental distribution images can reveal hidden sub-surface layers, including modifications made by the artist or restorations on the surface. In this way it can provide a unique insight into the creative process of the artist(s) and the painting's conservation history (Alfeld, Matthias, et al., 2013). Pigment identification is used by conservation scientists to elucidate artist/workshop use of materials, to understand how a painted surface has altered over time informing how an artwork is to be conserved, and lastly, to identify anachronistic uses of materials that could be associated with either fakes and forgeries or associated with past restoration. A primary tool for these tasks is macro X-ray fluorescence (MA-XRF), a non-invasive method that has become common place in cultural heritage to examine how elements related to various pigments are distributed across a painted surface. Recently, numerous instrument designs have been developed in an effort to cope with challenges associated with analyzing painted supports, for example, limited access to the object, and the high complexity and heterogeneity of the artifact at multiple scales (Pouyet, Emeline, et al., 2020). MA-XRF for the investigation of historical paintings was first described in the early 1990s, but the method found no widespread application until Dik et al. employed

it to visualize the study of a peasant's head underneath a painting that Vincent van Gogh created during his stay in Paris (Alfeld, Matthias, et al., 2013). Initially, MA-XRF has been mainly used to study easel paintings, but recently its scope has been broadened to other two-dimensional (i.e., 'flat') cultural heritage objects such as stained glass windows and illuminated manuscripts (Ricciardi, Paola, et al., 2016).

3.2.4 Working principles of MA-XRF

Being able to transport instruments and perform in-situ analysis is of utmost interest for cultural heritage scientists, seen that it's very unlikely that a priceless artwork will leave the tutelage of the museum save rare exceptions. MA-XRF investigations are performed by using an X-ray tube and one (or more) detector(s), acquiring one spectrum for each pixel throughout the sample surface. There are few different formats when it comes to the scanning geometry itself – besides the classical tube sample-detector geometry. First, whether the scanning head or the sample will move with the x-y motorized stage and second whether they will be positioned vertically or horizontally. Another critical point in the scanning systems is the beam focusing and detection efficiency. Two common choices for focusing the beam are pinhole collimators and polycapillary lenses, the former being a considerably cheaper option, but with the drawback of reducing the beam intensity and thus increasing the dwell-time (time spent on each pixel) (Lins, Sergio Augusto & Gigante, Giovanni & Cesareo, R. & Ridolfi, Stefano, 2019).

MA-XRF provides elemental maps that can be compared with great benefit to pictures recorded with different scientific imaging techniques using either X-rays with radiography, laminography, emissiography or neutrons with the neutron autoradiography, or eventually photons in the ultraviolet to infrared domains such as UV fluorescence, false colour infrared, IR reflectography, etc. Because of the high mass attenuation coefficient of lead, contrast in X-ray radiography is mainly reflecting lead white distribution, often present in the ground and the pictorial layers. As a consequence, the slight contrast induced in radiographs by lighter elements present in other pigments, e.g. copper, iron or manganese, is often obscured. In addition, when the preparation or the support is more absorbing than the paint layers (e.g. thick lead-white ground or wood panel support), X-ray radiography provides a poor image of the composition. Contrary to images obtained with X-rays in transmission mode, elemental images acquired in emission mode using MA-XRF are less affected by these

considerations and appear highly complementary to X-ray radiography. The ability of MA-XRF to image pigment distribution by means of their elemental signature may qualify it, in some sense, as 'colour radiography'. Such optimistic considerations must, however, be moderated, as MA-XRF presents important limitations. Firstly, the low XRF cross section of light elements and the absorption of X-rays by the varnish layer and the air between the painting and the detector generally prevent imaging of elements with energy lines below 2 keV (sulphur). Secondly, acquisition of maps with fine resolution can be very time consuming, often requiring days of operation. The acquisition of a satisfactory spectrum during the short time spent on each pixel (fraction of a second) requires the use of intense incident X-ray beams combined with high efficiency detectors able to stand large count rates. Finally, MA-XRF maps resolution is limited by the size of the X-ray beam. X-ray optics can be used to obtain small beams but maintaining the painting in focus of the system can be difficult if its surface is not flat. Commercially available XRF scanners for paintworks overcome these limitations, at the expense of complexity, weight and cost (multiple detectors, focusing X-ray optics) (Ravaud, E., et al. 2016).

Chapter 4. Acquisition operation system of MA-XRF

4.1 Translation stage and scanning head

Furthermore, the logistic and financial efforts of bringing a precious painting to a synchrotron radiation source are considerable and limit the number of paintings that can be investigated. In order to broaden the range of paintings that may be investigated, mobile MA-XRF instruments for in situ investigation of paintings were developed. In these instruments the X-ray tube and detectors are mounted on a motorized stage and moved before the surface of a (stationary) painting during a scan.

The pigments used to create a painting are generally present at a concentration level of several mass percent. By employing high intensity synchrotron radiation to scan the painting, the heavy elements present in the paint can be visualized with dwell times far below one second. However, also a well designed X-ray tube based system can be sensitive enough to image their distribution at a comparable pace. The main limitation of the system is the fact that, as an experimental system, it requires a highly trained operator. So a scanner for fast routine MA-XRF imaging of historical canvases or panel paintings was still missing. Characteristics of such a scanner would be: (a) capable (in terms of sensitivity and speed of the motorized stage) of acquiring the elemental distribution images of elements present at several mass percent with dwell times of less than a second; (b) easily transportable (by private car) between museums and galleries; (c) featuring a variable beam size to allow for overview (image resolution 0.5 mm) as well as detailed (resolution 100 mm) scans without changing the optic; (d) intuitive control software that allows the operation by a person trained, but not specialized in XRF analysis and/or imaging (Alfeld, Matthias, et al. 2013).

The prototype is composed of an exchangeable scanning head, a motorized X-Y stage with a controlling unit and a laptop. The scanning head can be easily changed between different X-Y stages to suit different needs. Within the current framework, two stages are operational. One, portable, for scanning areas up to 20 x 20 cm^2 and a larger, mobile one, for scanning areas up to 100 x 100 cm^2. The controlling interface (CI) was programmed in LabView and features an “almost live” display of the counts map and the last acquired spectrum. The same CI controls both small and large motorized stages, thus requiring a minimal effort to change from a portable to a mobile scanner following a plug-and-play approach. The developed system has been put to test with different materials of cultural science interest: gilt and painted leathers, painted copper plates,

corroded alloys, sediment blocks and canvas paintings (Lins, Sergio Augusto & Gigante, Giovanni & Cesareo, R. & Ridolfi, Stefano. 2019).

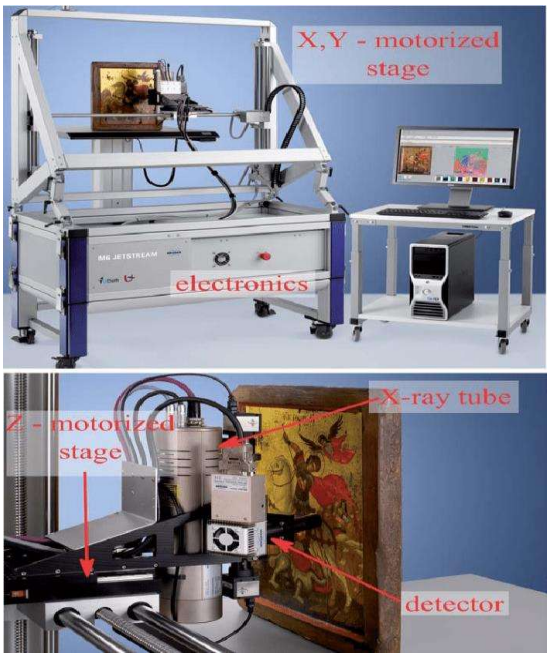

Figure 10. Bruker M6 Jetstream set-up and details of the measuring head

The M6 Jetstream consists of a measuring head that is moved over the surface of a painting by means of a X,Y-motorized stage(Figure 10).This motorized stage features a minimum step size of 10mm and a maximum travel range of 8060 cm (hv). By combining the elemental distribution images obtained by scanning sub-areas, objects larger than the maximum travel range of the motorized stages can be investigated as a whole: thus, it becomes feasible to scan medium sized paintings with dimensions of $32m^2$, for example. The exact distance between the measuring head and the painting is adjusted by a motorized stage of 7 cm travel range oriented along the Z axis. The measurement head travels within a metal frame that can be tilted in order to adjust it to the surface of a painting and to allow the analysis of horizontally positioned samples

The frame holding the motorized stage is mounted on a box containing the detector electronics, the motor control electronics and the high voltage generator of the X-ray

tube. The electronics box itself is mounted on a wheeled platform that allows for easy transport over short distances and positioning with respect to the painting. For transport the measuring head can be demounted and stored in the electronics box; the wheeled platform, the electronics box and the frame holding the motorized stage can be separated (Alfeld, Matthias, et al., 2013). The XY scanning is performed in a continuous movement of the X axis with a maximum speed of the scanner 100 mm/sec. The Y step is selected by the user initially. The scanner is so designed for making ultra-fast scans covering the total area in 4.2 hour with a lateral resolution of 500 μm. The Z-axis enables the sample movement with high accuracy along the beam focal direction (Caliri, Claudia, 2017).

The measurement head is moved during the scanning by means of a custom designed three-axis system. It consists of three linear stages allowing a travel range of 110 cm, 70 cm and 20 cm along the X, Y and Z directions, respectively. Wire sensors are integrated in each of the axes for measuring the absolute position of the measurement head in XYZ coordinates. This technical solution in place of conventional inductive proximity switches used in commercial stages allows avoiding any referencing of the axes before starting a new measurement. The system can be switched on/off and the value of the position is always available; in this way a measurement can be restarted from the same position when it is interrupted for any reason (i.e., during the closing time of a Museum). The Z axis is used for positioning the sample at the measurement distance before starting a new scanning. Moreover, data provided in a live mode by the laser sensor can be used to dynamically correct the Z position during the scanning in order to maintain the measurement head at a uniform distance from the sample (Romano, Francesco Paolo, et al., 2017).

4.1.1 X-ray optics

Polycapillary optics have gained broad acceptance and now are being used in a wide variety of applications. Beginning as optics integrated into research setups, they were used to enhance the performance of existing X-ray analytical instruments, and are now widely used as essential components in X-ray spectrometers designed to utilize the optics capabilities (Gibson, David, and Walter Gibson, 2002).

Polycapillary optics are arrays of small hollow glass (monocapillaries) tubes. X rays are guided down these curved and tapered tubes by multiple reflections in a manner analogous to the way fiber optics guide light. They differ from single-bore capillaries and X ray mirrors in that the focusing or collecting effects come from the overlap of the beams from thousands of channels, rather than from a few surfaces. Generally, this results in relatively efficient collection, especially from large divergent sources such as conventional X ray tubes, but does not produce submicron beam spot sizes. In several cases, high intensities of the primary beam are needed for the detection of low concentration elements. Further, the use of optics allows to perform local analysis at high spatial resolution (e.g., below 100 μm) (MacDonald, Carolyn A., 2010).

A principle benefit of polycapillary optics is the ability to capture X-rays from a divergent source over a large solid angle and to redirect them by multiple external total reflections into a quasiparallel or focused X-ray beam (Gibson, David, and Walter Gibson., 2002).

Polycapillary optics can operate in focusing and collimating modes by gently bending the capillaries to an appropriate curvature.

The most characteristics of a polycapillary X-ray lenses are below:

- **Input focal distance** (IFD): To define where the X-ray source is to be placed
- **Output focal distance** (OFD): To define where the smallest beam size is obtained

  A polycapillary focusing optic can focus the X-rays to a spot size as small as 5μm (at Rh Ka radiation, 20.2 keV). The X-ray flux density obtained at the focus of the optic can be up to five orders of magnitude higher than that obtained with a conventional pinhole collimator. This level of X-ray flux density improvement has been a game-changer for micro X-ray fluorescence.

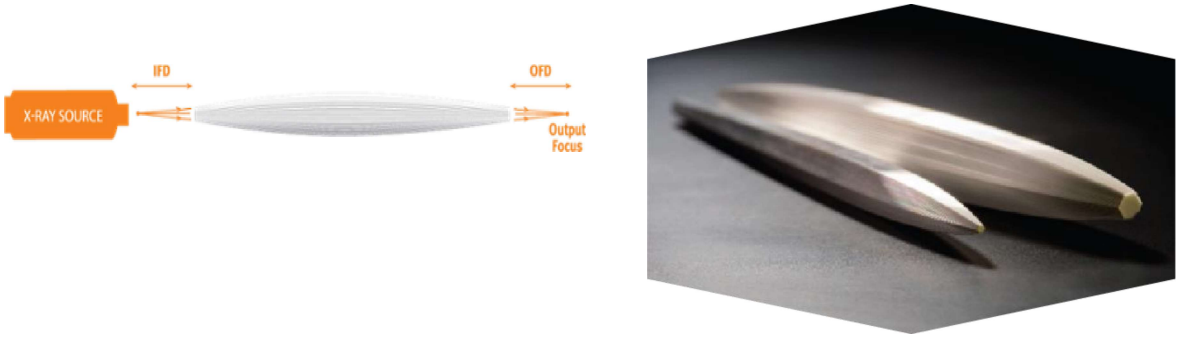

Figure 11. Focusing X-ray Optic (photo by XOS website)

Focusing Monolithic Optics

– Point to point focusing

– Small focal spots • < 25 μm @ Cu Kα • < 15 μm @ Mo Kα

– Capture angle: up to 20°

– Transmission efficiency: up to 30 % (geometry and energy dependent)

A polycapillary collimating optic, with the output beam diameter as large as 25mm, can generate a quasi-parallel X-ray beam for applications such as X-ray diffraction (XRD) and wavelength dispersive spectrometry (WDS). Depending on the X-ray energy, the collection solid angle of the optic can be up to 40° and the transmission efficiency can reach 40%.

Collimating Optics

• Multifiber

– Output beam size: 10 x 10, 20 x 20, 30 x 30 mm2

– Output divergence: ~ 4mrad CuKα

– Capture angle: 4.2°, 7°, 8.8 °

– Axial and planar divergence are identical

– Up to 30 % transmission efficiency

• Monolithic

– Output beam size diameter: 0.5mm, 1.5mm, 4mm, 6mm

– Output divergence: ~1 mrad MoKα, ~2 mrad CuKα

– Capture angle: up to 20 ° – Transmission efficiency: up to 30 % (geometry and energy dependent) (Gibson, David, and Walter 2002)

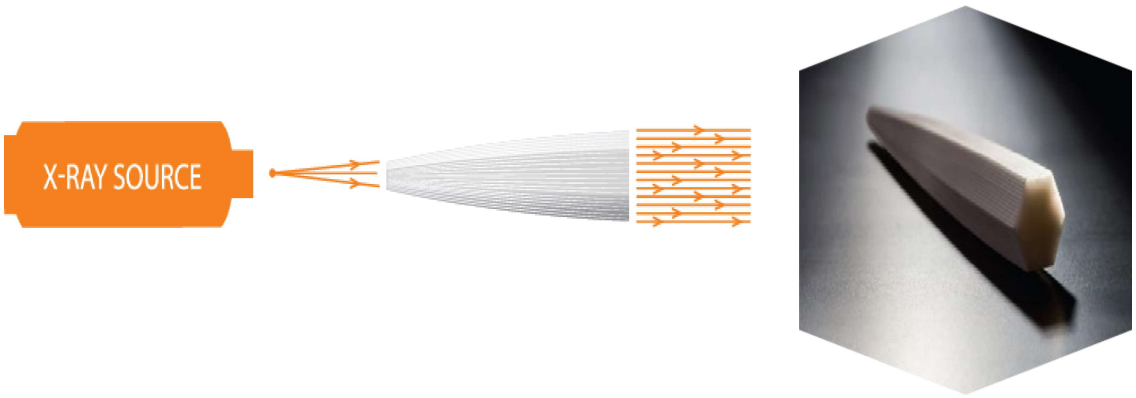

Figure 12. Collimating X-ray Optics (photo by XOS website)

4.2 Detector

The detection of fluorescence is based on the conversion of the energy released by a photon in the detector material into an electrical signal. The preferred detectors in X-ray spectroscopy are the semiconductor detectors. Their main advantages are due to high detection efficiency and high energy resolution. This aspect is related to the fact that, the mean energy needed to create one primary elementary charge is of few electron volts (3.62 eV for Silicon), ten times lower than others X-rays detectors (scintillators and gas detectors). In this way, the energy/charge conversion factors, i.e. the number of charge carriers generated for a given energy is higher for semiconductors than for other detectors, leading to a much smaller statistical broadening of the fluorescence peaks.

4.2.1 Detector efficiency

X-rays release their energy in the detector crystal through the interaction mechanisms of the X-radiation with the matter: photoelectric effect, Compton Scattering and Rayleigh scattering, of which processes the energy and atomic number dependence. Detection efficiency expresses capabilities of a detector. It is defined as the fraction of the total number of photons emitted by the source, which interacts in the detector volume and that are absorbed completely. It is formalized by the product of the following terms:

$$\eta = \eta geom \cdot \eta i \cdot \eta photo \quad (1)$$

where:

i. geometrical efficiency ($\boldsymbol{\eta geom}$), the fraction of the photons emitted by the source which enter the detector volume. It takes in account the active area of the detector and the distance with respect to the source.

ii. intrinsic efficiency ($\boldsymbol{\eta i}$), the fraction of photons entering the detector, which interact in the detector material (Knoll, Glenn F. John Wiley & Sons, 2010). Whereas for the intrinsic efficiency of a given detector, it can be easily calculated in basis of the detector material and its thickness. The efficiency is given in number of photons that interacts with the detector according to the Beer-Lambert equation:

$$I = I0e\ -\mu(E)\rho w \quad (2)$$

Where I is the portion of photons after crossing a sample of density ϱ and mass attenuation μ, for a given incident energy E and with thickness w of an incident beam of intensity I0. Moreover, the detector window will also absorb some of the incoming radiation. This effect can be as well estimated by the Beer-Lambert equation, and the combination of intrinsic efficiency and window efficiency can be referred to as quantum efficiency (Lins, Sergio Augusto Barcellos, 2018).

iii. photo-peak efficiency ($\boldsymbol{\eta photo}$), the fraction of the photons interacting in the detector, which deposit their full energy in the material (Knoll, Glenn F. John Wiley & Sons, 2010).

The energy of the escape peaks is equal to the difference between the incident photoelectron energy and the scape photon energy. This effect is negligible for energies above 10 KeV but, when dealing with lighter elements, this effect plays an important role. Because of that, the escape fraction, i.e. the amount of escape photons, can be calculated and is useful when applying corrections to the spectrum during the quantification step (Lins, Sergio Augusto Barcellos, 2018).

Another effect caused by the action of the detector is the pileup effect, which results in sum peaks within the spectrum. This happens when two photoelectrons enters the detector within a time interval too short for the detector to process them, resulting in a "recognized" signal with an energy corresponding to the sum of the two photoelectrons involved in the process. Sum peaks are hardly misinterpreted as another chemical

element, meaning they will not strongly affect a qualitative analysis. In the other hand, for quantitative analysis, the appearance of sum peaks may change the observable abundance of one or other element, making it fundamental to correct this effect, often mathematically. Changing analysis conditions (by the use of filter or lowering the counts per second – cps) can also help counterbalance these effects. There are, of course, other effects that can cause alterations on the spectrum (often hard to quantify). The collection of photons by the detector follows a Gaussian distribution and is a statistical process. The peaks are shown in the spectrum as an approximate Gaussian distribution due to the photon-to-charge conversion that takes place within the detector and the electronic noise caused by the amplification of the signal. An incomplete charge collection can cause disturbances on the lower energy part of the spectrum, representing the 19 apparent continuum in this region to be higher than expected. This effect is caused by intrinsic defects of the detector such as dead layers and low electric field regions (Lins, Sergio Augusto Barcellos, 2018).

4.2.2 Energy Resolution

In spectroscopy, an important requirement of a detection system is the capability of the system to distinguish photons closely separated in energy. The energy resolution is commonly expressed as full-width-at-half-maximum (FWHM) of the measured distribution. Alternatively, it can be expressed as percentage R, defined as the ratio between the FWHM and the centroid value of the distribution:

$$R = \frac{\Delta E_{FWHM}}{E_0} \quad (3)$$

The measured distribution can be described by a Gaussian function, whose expression is given by:

Detectors

$$G(E) = \frac{N_0}{\sigma\sqrt{2\pi}} \exp\left(\frac{(E-E_C)^2}{2\sigma^2}\right) \quad (4)$$

with σ the standard deviation, N0 the peak area, and Ec the peak centroid. For a Gaussian distribution the FWHM results related to the σ as $FWHM$ = 2.35 σ. Several noise sources limit the energy resolution of detector and contribute to the broadening of the peaks. In particular, for semiconductors, the $\Delta EFWHM$ (or standard deviation σ) includes:

i. statistical noise related to the conversion process of the photon energy into charge carriers.
ii. electronic noise of the detector–amplifier system.
iii. collection noise related to the partial collection of the signal charge.

$$\Delta E^2_{FWHM} = \Delta E^2_{statistical} + \Delta E^2_{el.noise} + \Delta E^2_{collection} \quad (5)$$

For semiconductors, statistical noise is expressed through the Fano factor (F):

$$\Delta E_{statistical} = 2.35\sqrt{(FE\varepsilon)} \quad (6)$$

where E is the photon energy and ε is the average energy needed for the pair electron vacancy production. The Fano factor is 0.11 for silicon crystal detectors (Guerra, M., et al 2012).

4.2.3 SDD Detector

Silicon Drift Detectors (SDD) have been used for collection fluorescence radiation. In recent years, their use has been grown compared to the more conventional planar detectors (Si(Li) and Si-pin detectors).

In the SDD, the charge is drifted from a large area into a small read-out node with low capacitance. Thus, the serial noise decreases and shorter shaping time can be used. This offers two advantages, first faster counting is enabled and at the same time, higher leakage current can be accepted, drastically reducing the need for cooling. Presently, SDD at room temperature achieves an energy resolution of the order of 180 eV4A consequent next step on the path to higher energy resolution was the search for "materials" with even lower "ionization" energy. The electrons of superconductors bound in Cooper pairs are such a material. The binding energy of the Cooper pairs is of the order of a few millielectron volts. Thus about 1,000 times more charge is generated per absorbed energy. This charge can be detected with a super conducting tunnel junction (STJ), a Josephson contact where the super conducting Josephson current is suppressed by a magnetic field. Potentially, the resolution limit should be about 30 times lower as compared to semiconductor detectors. Energy

resolution in the range of 12 eV for manganese x-rays (6 keV photon energy) has, indeed, been demonstrated , comparable to the early liquid nitrogen cooled systems, with shaping times of 250 ns. A detailed discussion of these detectors is given in the first section of the chapter. In the second section, the perspective of a combination of energy and spatial resolution using silicon detectors is discussed.

Originally designed as position-sensitive detectors for particle tracking, silicon drift detectors are nowadays used for high-count-rate X-ray spectroscopy, operating close to room temperature. Due to their low-capacitance read-node concept, they are among the fastest high-resolution detector systems. They have opened a new spectrum of experiments in the wide field of X-ray spectroscopy: fluorescent analysis, diffractometry, material analysis, synchrotron experiments and X-ray holography. In addition, the detection of visible light, near-infrared light and UV light is measured with high efficiency. The low-noise readout of the light of scintillation crystals extends the spectrum of possibilities to the hard X- and gamma-ray spectrum. The fact that the detector system can be used at room temperature with good spectroscopic performance, and at–10C with excellent energy resolution, avoiding liquid nitrogen for cooling and high-quality vacuum, guarantees a large variety of new applications, independent of the laboratory environment (Strüder, L., P. Lechner, and P. Leutenegger,1998).

Silicon Drift Detectors (SDD) have been used for collection fluorescence radiation. In recent years, their use has been grown compared to the more conventional planar detectors (Si(Li) and Si-pin detectors). They offer higher performance in term of lower electronic noise at very short peaking times. This provides a better energy resolution at moderate count rates and much better energy resolution at high-count rates. The main components of a SDD detector are (Guerra, M., et al. 2012):

1. Collimator assembly
   The collimator provides a limiting aperture through which X-rays must pass to reach the detector. This ensures that only X-rays from the area being excited by the electron beam are detected, and stray X-rays from other parts of the microscope chamber are not included in the analysis.
2. Electron trap

Electrons that penetrate the detector cause background artefacts and also overload the measurement chain. The electron trap is a permanent magnet assembly that strongly deflects any passing electrons. This assembly is only required on detectors with thin polymer windows, as thicker beryllium windows efficiently absorb electrons below 20 keV in energy.

3. Window

   The window provides a barrier to maintain vacuum within the detector while being as transparent as possible to low energy X-rays. There are two main types of window materials. Beryllium (Be) is highly robust, but strongly absorbs low energy X-rays meaning that only elements from sodium (Na) can be detected. Polymer-based thin windows can be made much thinner than Be windows and therefore are transparent to much lower energy X-rays, many allowing detection of X-rays down to 100 eV. Although these window materials are far less robust, by placing them on a supporting grid they can withstand the pressure difference between the detector vacuum and a vented microscope chamber at atmospheric pressure. The greater transmission of the polymer-based windows means that they have largely replaced Be as the material used for detector windows. In instruments that operate under very high vacuum conditions, for example TEMs, it is possible to use windowless detectors which allow for even more sensitivity for light elements.

4. The sensor

   The sensor is a semiconductor device that through the process of ionisation converts an X-ray of a particular energy into an electric charge of proportional size. Two main types of sensors are used for X-ray detection: traditional silicon crystals drifted with lithium, so-called 'Si(Li)', and newer faster Silicon Drift Detectors ('SDD') which have largely replaced them. SDD devices use a field gradient applied by ring electrodes on its back surface to collect the charge liberated by each X-ray detected, at the anode. The silicon drift detector (SDD) sensor is fabricated from high purity silicon with a large area contact on the entrance side facing the incoming X-rays. On the opposite side there is a central, small anode contact, which is surrounded by a number of concentric drift electrodes

5. The FET

The field effect transistor (also known as the FET), is connected directly to the sensor. It is the first stage of the amplification process that measures the charge liberated in the crystal by an incident X-ray and converts it to a voltage output.

6. Detector cooling

SDD detectors operate at a few tens of degrees below zero and are cooled by Peltier (thermoelectric) devices bound to the SDD sensor. Heat from these devices is transferred to cooling fins in the body of the detector, by a cold finger or heat pipe, where it is dissipated.(Oxford instruments plc., 2012)

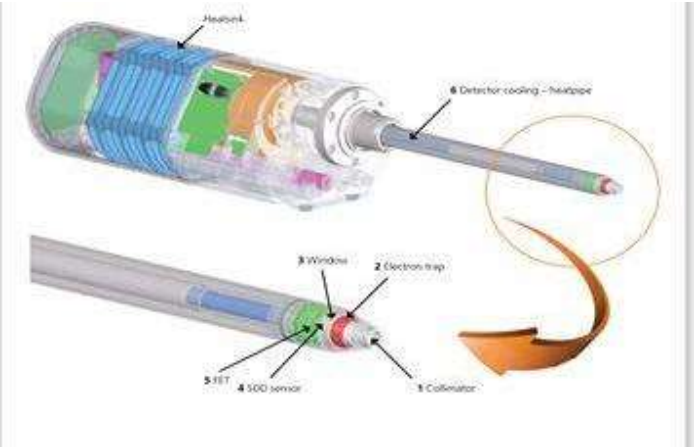

Figure 13. Cutaway diagram showing construction of a large SDD detector

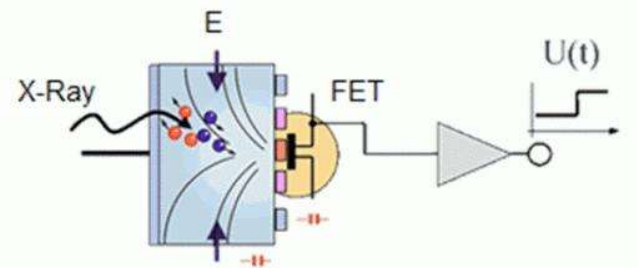

Figure 14. Cutaway diagram showing construction of a large SDD detector

The working principle of a SDD detector is schematized in Figure 14. It consists of a three stage process: (1) the photon energy conversion into a charge by the ionization of atoms in the semiconductor crystal, (2) the charge conversion into a voltage signal by the FET preamplifier, (3) the voltage signal is taken as input into the digital signal processor (DSP).

Differently from conventional detectors with planar structure and uniform electric field between anode and catode. The SDD technology is based on a cylindrically symmetric structure with a radial electric field, as is showed in Figure 14. The anode is a small circle and the drift electrodes are annular. The small area of the anode translates in a very small capacitance. The active volume can be enlarged by adding more electrodes keeping the same anode area. This technology allows to reduce the voltage noise proportional to the anode capacitance and provides a better energy resolution especially at high-count rates (Guerra, M., et al., 2012).

The system is fully controlled by a custom programmed control unit (CU). The CU allows the real-time control of all sensors in the device providing safety restriction for the samples during the scanning; it collects X-Ray events and builds XRF spectra based on user inputs. Finally, the CU provides elemental distribution images by processing in a live mode the X-ray pixel spectra with the fast fitting plugin developed for PyMca and integrated in the system (dos Santos, Hellen Cristine, et al., 2018).

Chapter 5. PyMca data processing and data collecting

5.1 Spectrum analysis

5.1.1 Spectra evaluation

The aims of spectrum evaluation is to extract analytically relevant information from experimental spectra. Obtaining this information is not straightforward because the spectral data are always corrupted with measurement noise. Fitting an appropriate mathematical function to the spectral data can do this. The fitting function generally consists of two parts, one that describes the continuum and one that deals with the characteristic lines (Van Grieken, Rene and Andrzej Markowicz, 2001).

XRF spectra consist of overlapping fluorescence lines of the elements present in the sample and of the spectral background due to the scattering of the primary radiation and the incomplete charge collection in the detector. Thus, if the escape and sum peaks are neglected and the spectral background is assumed to be of constant shape, a spectrum S can be described by a function yi in channel i as in equation:

$$y_i = C_0 B_i + \sum_{K=1}^{k} C_K x_{i,k}(a_0, , a_1, a_2, \dots a_m) \quad (7)$$

where B is the spectral background, k the peak profiles and x represent appropriately grouped transitions in the excited atom. Their shape is dependent on the non-linear variables a that contains the energy calibration and resolution of the detector and other characteristics of the spectrometer. The peak intensity is expressed in the linear factor c. In elemental distribution images the color intensity of a pixel is directly correlated to this factor.

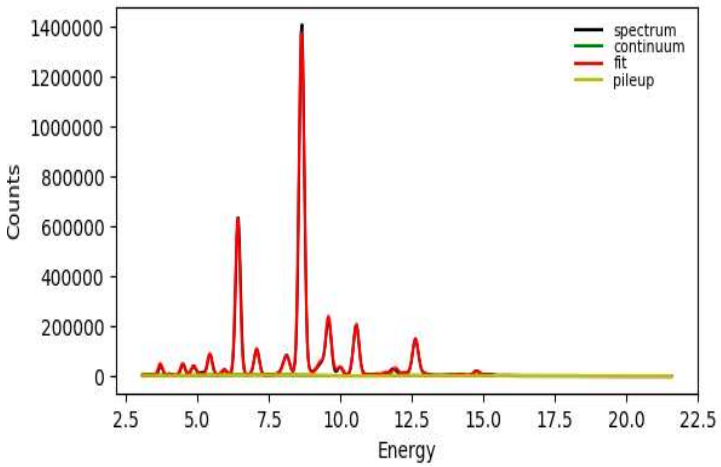

Figure 15. XRF spectrum fast fitting performed using PyMca software of analyzed painting

In order to discriminate the overlapping fluorescence peaks and to derive the area of each peak, the individual components are modelled using mathematical functions, based to the knowledge of the fundamental parameters theory. Fitting a mathematical function to n experimental data (x_i , y_i) consists in determining the optimum set of m parameters (a_0 a_1 a_2 ….. a_m) such that the computed values with function f (x_i,a) will be a close as possible to the experimental values yi .The different parameters of the fitting function are obtained by the *non-linear least-squares method* (NLLS) the same approach is followed for processing XRF spectra (Van Espen, P., H. Nullens, and F. Adams., 1977).

Generally, if Φ is the function to minimize:

$$\phi = \sum_{i=0}^{n} \left(\frac{f(x_i;a)-y_i}{\sigma_i}\right)^2 \quad (8)$$

Where σ_i is the standard deviation of experimental value y_i . The parameters values are obtained by minimization of Φ, i.e. by cancelling out the values of its partial derivatives:

$$\frac{\partial \phi}{\partial a_j} = 0 \quad (9)$$

In the fast linear fitting procedure used in the MA-XRF this minimization is performed by using the Marquardt-Levenberg algorithm. This is based on two different approaches as fitting progresses: far from the minimum, the gradient method is first used, then, when near the minimum, it is replaced by the Hessian method.

In both cases, solving the equation system requires computation of the first derivative for each of m parameters. Uncertainties (variances) associated to each parameter are calculated during the fitting procedures, as well as covariances of the different parameters. A complete description of the algorithms and the theoretical databases on which is built the fitting procedure can found in references

5.1.2 Peak shape model

The response function of most solid-state detectors is predominantly Gaussian, thus common kinds of spectra, gamma, alpha or X-rays are modelled on Gaussian function:

$$\boldsymbol{G(x) = \frac{A}{\sigma\sqrt{2\pi}} \cdot exp\left[-\frac{(x-x_0)^2}{2\sigma^2}\right]} \quad (10)$$

Gaussian peak is characterized by three parameters: the position x_0, amplitude A, and standard deviation σ. It is preferable to describe the peak in terms of its area rather than its height because the area is directly related to the number of X-ray photons detected, while the height depends on the spectrometer resolution. The peak area, in equation (9) is a linear parameter; the width and position are non-linear parameters. This implies non-linear least squares procedure, described above, in order to find optimum values for the latter two parameters. Instead of a Gaussian function, in certain instances it may be necessary to resort to more complicated models such as Voigt or Hypermet functions. In particular, this latter is used in the XRF spectra analysis of this work. The Hypermet fitting function was first introduced by Philips and Marlow (Sole, VA, et al. 2007) and it consists in the sum of a Gaussian, a low-energy tail and a discontinuity centred on the peak position:

$$\mathrm{f}_{Hypermet}\ (\mathrm{x}) = \mathrm{G}(\mathrm{x}) + T(x) + S(x) = TG(x) + S(x) \quad (11)$$

The Gaussian tail T(x) in equation is modelled by an exponential function truncated at the peak position, convolved with a Gaussian representing the instrumental broadening. This shape can be used to take into account events due to incomplete charge collection in the detector.

$$T(x) = \int_{-\infty}^{x_0} A \cdot T(\tau \cdot x') \cdot exp\left[-\frac{(x'' x_0)^2}{2\sigma^2}\right] dx' \quad (12)$$

$T(x)$ function includes two more parameters to the Gaussian function G(x): tail relative amplitude T and exponential slope τ. The discontinuity (x) results from the convolution of a step function, with a constant value for $x \leq x_0$ and zero value for $x > x_0$, by the Gaussian instrumental broadening . Mobile scanning MA-XRF

$$s(x) = \int_{-\infty}^{x_0} A \cdot S \cdot exp\left[\frac{(x''-x_0)^2}{-2\sigma^2}\right] dx' \quad (13)$$

The function $S(x)$ is entirely characterized by six parameters, the first five are the same as those of the Tailed Gaussian $TG(x)$ and the last one is S the step function relative amplitude spectra (Van Espen, P., H. Nullens, and F. Adams, 1977).

In Gaussian equation the peak area is a linear parameter; the width and position are non-linear parameters. This implies that a non-linear least-squares procedure is required to find optimum values for the latter two parameters. Linear least-squares

fitting methods can be used assuming the position and width of the peak are known with high accuracy from calibration (Sole, VA, et al., 2007).

5.1.3 Continuum/Background evaluation

The continuum is modeled in two possible ways: estimation or fitting. In the former, the estimated background is subtracted from the experimental data prior to the least-squares fitting of the fluorescence peaks. In the fitting mode the continuum is described by an analytical function which enters into the least-squares fitting algorithm. PyMCA implements both models.

Background can be estimated thru an iterative procedure in which the content of each channel is compared against the average of the content of its neighbors at a distance of i channels. If the content is above the average, it is replaced by the average. In order to speed up the procedure, i can be taken as a fraction of the peaks full-width-half-maximum (FWHM) at the beginning of the iterative process, being one at the end of it. An optional Savitsky–Golay smoothing at the beginning of the process is possible as recommended.
The analytical functions currently supported to describe the background are polynomials of user selectable degree on

$$x = (E - E_{mean}) \text{ or on } x = \exp(E - E_{mean}) \quad (14)$$

where E is the energy of the considered point of the spectrum and E_{mean} is the energy at the center of the fitting region (Sole, VA, et al. 2007).

5.2 PyMca data collecting

A control panel allows to enable a new analysis: X-ray data, that are accumulating during acquisition, are read and analyzed line-by-line. The software converts the raw-data format into EDF format (European synchrotron radiation facility Data Format) and a suitable fitting model is applied to the spectra, allowing the simultaneous creation of images (Solé, V. A., Papillon, E., Cotte, M., Walter, P., & Susini, J., 2007) The setup of the configuration parameters of the fit had to be as simple as possible. This practical requirement led to the development of a complete visualization and data analysis tool named PyMca (Python multichannel analyzer). This application relies on the Python bindings to the C++ programming toolkit Qt and the library Qwt to build its platform independent graphical interface and plotting routines. Nevertheless, the fitting code can run in prompt or batch mode fully independent of any graphical package region (Sole, VA, et al. 2007). PyMca is based on the same mathematical routines as AXIL and features next to a modern GUI for XRF fitting and image manipulation many convenient tools. It provides a ROI imaging tool, which allows for the interactive inspection of data with a range of useful plug-ins and it contains the selection of

mathematical functions for peaks and background shapes, the experimental conditions (excitation type, detector specifications, measurement geometry), the energy calibration and the fluorescence peaks composing spectrum. Fitting procedure separates so the several spectrum components and gives as result the net area of each fluorescence peak. In this way, the net counts image (of float image) is created line-by-line repeating the procedure, until the completion of the entire map, its running can be visualized in the same panel. The analysis running speed is more than 5000 spectra/sec as maximum processing speed. The pixel size of images can be changed during analysis using the same control panel, if images are not satisfactory in terms of lateral resolution or counts statistic.

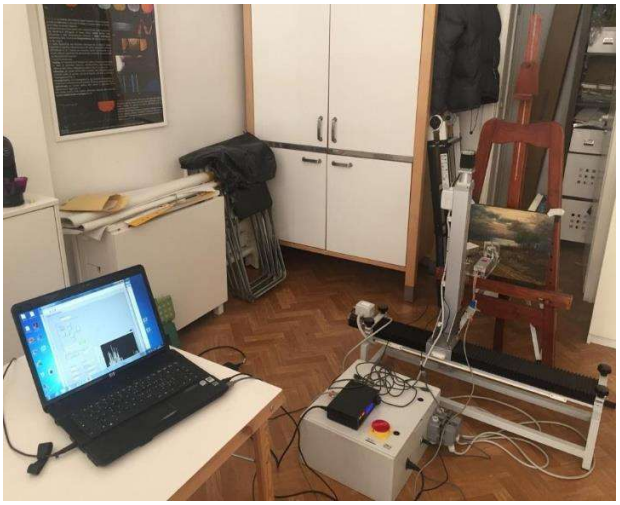

Figure 16. Analysis software in running on a laptop connected to Control Unit

Analysis software is also supplied with a second panel "image editing", for the images elaboration. This control panel allows the image graphical processing during or at the end of imaging procedure. Intensity (or float) maps are converted in 0-255 range grayscale images, having the possibility to change graphical settings as colormap, contrast and brightness, resizing, etc. In addition, arithmetic and logical operations can be applied to the images for subtracting noise or contaminations and also eventual systematic shift correction can be done. However, shift pixel effect occurs especially when a fast acquisition is performed as result of a systematic errors between axes sensors and acquisition system (Anitha, A., Brasoveanu, A., Duarte, M., Hughes, S., Daubechies, I., Dik, J., ... & Alfeld, M. 2013).

To do research the MA-XRF scanning was performed with a portable prototype scanning system built in a private company, Ars Mensurae. The system features an exchangeable and modular scanning head and different X–Y scanning stages. The head components used for the present analysis were: one low-power (4W) Moxtek® Ta-target tube (collimated to 1 mm) and one AMPTEK® 123SDD detector having an active area of 25 mm^2 and a thickness of 500 μm. The energy resolution is of 125 eV @ the Mn-Kα line (5.9 KeV). The scanning stage used was the smaller, portable version, capable of holding samples up to 200 × 200 mm^2 in dimension. The total scanned area was 80×40mm^2 and the dwell-time was 3s. Tube voltage and current were set to 35 KV and 17 μA, respectively (Barcellos Lins, Sergio Augusto, et al. 2020).

Chapter 6. Results and discussion

To plan the preservation treatment of a painting one needs to evaluate its current state. This includes the identification of the materials used and the structural integrity of the painting. The earlier a defect is known, i.e. before it becomes visible on the surface, the better and easier it can be treated, sometimes just by adjusting storage conditions. In general as much of the painting's original structure as possible needs to be preserved. So it is of high importance to clearly discern between the painting's original structure and later additions, e.g. from previous restoration treatments.

Easel paintings are created by superimposing layers of paint, often achieving optical effects by letting covered layers shine through thinly applied top layers. Thick paint layers are completely opaque, so that "repented" elements of a painting can be corrected by overpainting. These changes are called pentimenti (from the Italian for verb pentire: "to repent") and their identification and visualization, next to the visualization of the initial sketch, are key elements in the revelation of changes to the initial concept.

The classical method of investigating a painting is visual inspection with different types of illumination and the aid of a stereomicroscope. This approach is in general limited of the surface, although in cracks of the surface sometimes hidden paint layers can be observed. In order to study hidden layers, samples from (preferably damaged) spots on the painting are taken. These samples are embedded in resin and polished to provide cross-sections through the painting's stratigraphy. In order to preserve the paintings original structure, the number of samples taken from a painting for scientific analysis has to be limited to a minimum and might be completely prohibited.

It is desirable to study the sub-surface features of paintings in a nondamaging and non-invasive manner. Also the transport of easel paintings should be avoided, as it asks for considerable financial and logistic effort and exposes the painting to unnecessary stress from handling and changing climatic conditions. For this reason in-situ techniques are the preferable means of investigation (Alfeld, Matthias, and José AC Broekaert, 2013).

6.1 The structure of easel paintings

The scientific investigations of easel paintings described in literature are in general focused on those created in the period from the Middle Ages until the end of the 19th century. A complete description of painting materials and techniques is far beyond the

scope of this topic, so that information will be limited a very general description, highlighting components relevant in the discussion below.

As seen in figure 17 an easel painting consists typically of a support, ground, paint layers and varnish that are applied on top of another. Canvas and wooden, panels are the most popular supports, but also other materials, such as thin copper plates, paper, stone, glass and even obsidian are known. The material of the support has a significant influence on the applicability of transmission methods. Further, the preservation of the support is crucial to preserve the structure of a painting and its investigation can reveal key information on the painting's history.

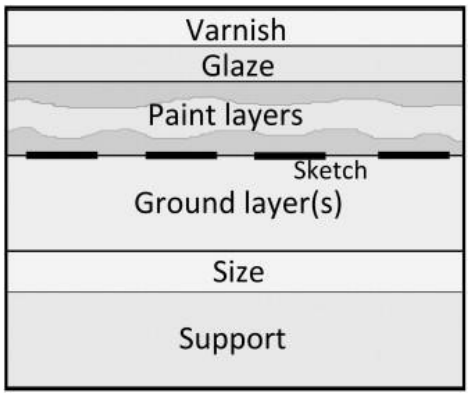

Figure 17. Schematic stratigraphy of an easel painting

A canvas support is prepared by stretching it on a frame before applying the ground layer. This results in cusping, scalloping of the regular weave pattern along each stretched edge, which is preserved in the canvas structure after the ground has dried. The absence of a complete cusping pattern on all sides of the painting can indicate a later modification of the painting's format. However, if a large canvas was prepared and cut for the creation of several paintings, as it is typical for industrially prepared canvas, the absence of a cusping pattern is to be expected. The earliest possible date of a panel paintings creation can be determined by dendrochronology of the support, if a characteristic year ring pattern can be observed in the accessible part of the panel. The direct access to the paintings support is often obstructed. Canvas loses its strength with time, so that it is sometimes stabilized by lining, i.e. gluing it on a second canvas, preventing direct observation of the canvas weave pattern, fibres and stamps on the back of the original canvas. Wooden panel supports were often stabilized by a

wooden cradle fixed to their backside in order to reduce the expansion and shrinkage due to changed temperature and humidity that results in stress and cracks in the paint layers, obstructing the direct access to parts of the panel's backside. The surface of canvas is commonly sealed with a water based glue size, in order to protect it and prevent the absorption of the ground's organic medium in the support. On the prepared support the first ground layer is applied. It provides a smooth surface to execute the painting on. The materials commonly used are chalk, gypsum, earth pigments and lead white in a glue or oil medium, but also quartz has been found in 17th century paintings. While before the end of the 16th century white grounds were common, later artists often used colored grounds. The color is achieved by the addition of pigments to the ground itself. In case of panel paintings, a similar effect can be achieved by the application of a second thin ground layer on the first ground, called imprimatura, which also smooths the surface of the ground. Colored grounds, commonly of grayish to reddish color, can be used in the n mid-tones of the painting, either by being left exposed or allowed to shine through the surface paint layers. The ground layer is seldom subject to imaging experiments as it covers the whole support and can be easily studied in micro-samples taken from the edge of the painting. Many artists sketch their initial concept directly on the ground of the painting. This is commonly done as an under-drawing, employing charcoal, chalk, metal point, ink or water-based black paint, or as an underpainting, defining main forms and principal shadows with brownish paint. The later was typical if a colored ground was employed and contributed to the final appearance of the painting if covered by thin paint layers. The sketch can either be made on the ground itself or on the imprimatura (Alfeld, Matthias, and José AC Broekaert. 2013).

The painting “Il Contadino” is shown in figure 18. It is an oil painting on a canvas panel of 32x37cm, belonged to private collection since XX century collection in Italy. Painting is from end of XIX century and attribution is under study. It was investigated elemental analysis with MA-XRF instrument.

Figure 18. "Il contadino" 19th century oil on canvas under normal light

Continuous scans were performed along the X direction at a scanning speed of 50mm/sec and with a fixed step-size of 500 μm along the Y direction. These parameters correspond to a dwell time per pixel of 10ms. The bottom part of the painting was investigated at 100 mm/sec along X. The pixel size of the mapping for the bottom part was 500 μm (dwell time per pixel 5ms). The time for covering each top sub-part was about 2 hours. Fig.19. shows the mosaic of all subareas in a RGB composite image (red - Zn: blue- Cr: green- Fe) distinguishing between the upper and central part.

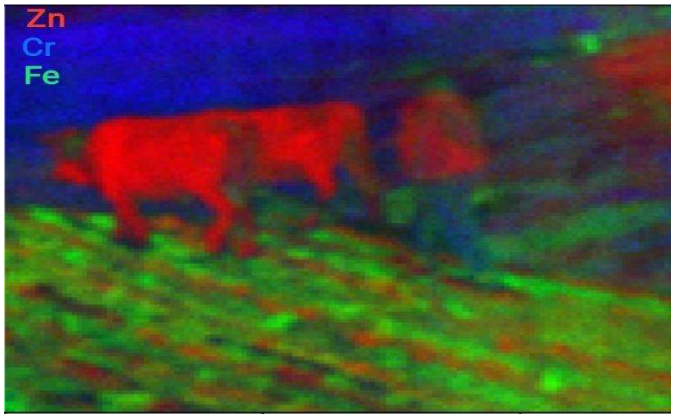

Figure 19. RGB composite image of the interest area of painting subdivided three areas

The painting was positioned at a distance of about 1.5 cm from the spectrometer head, corresponding to a beam size of 500 μm. The high resolution images were elaborated in

real time by using the PyMca software. The dynamic correction of the sample distance was not operated due the small curvature of the canvas. However, the laser system has been used during scan for controlling the preconfigured safe distance (0.8 cm) of the painting from the instrument. Ta target material was used as a X-ray tube. The detection system parameters were selected at 1.5 μs peaking time and 0.2 μs flat top, corresponding to an energy resolution of 160 eV. In figure 20. showed the MA-XRF scanner in execution.

Figure 20. MA-XRF instrument on "Il contadino" painting (photo by Stefano Ridolfi)

Our main interest area was focused on farmer part of painting which has more various colors have rather entire part. As it is shown below region of interest (ROI) painting under normal light image (Fig. 21.) and grayscale image. Grayscale image is more suitable to see hidden layers of painting obviously. The analysis of the "Il contadino" was performed on the fly by applying a full fitting procedure integrated in the software of the PyMca.

Figure 21. ROI image under normal light and grayscale mode

110x130 matrices were used to create local spectra in PyMca software (Fig. 21.) in addition to, local spectra were taking using ROI tool available in this program in order to simulate punctual XRF measurement, applied to the spectral dataset to investigate some inconsistencies in the data. This experimental approach evidenced the elements in the different pigments composing the artwork. The sum spectrum obtained during the scanning of the painting surface allowed identifying twenty five chemical elements: K, Sc, Ca, Ti, Cr, Mn, Fe, Ni, Cu, Ga, Zn, Sr, Sn, Ba, Hg, Hf, Ta, W, Pt, Au ,Pb, Br and Xe. However for fitting of spectra used these all elements, for pigment identification Fe, Cr, Pb, Zn, Ca, Ba main elements will be discussed in this work.

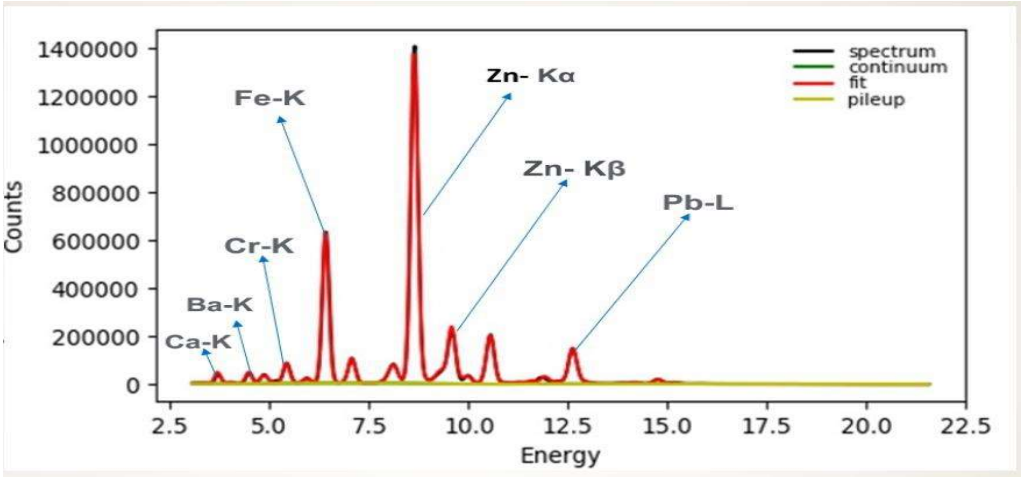

Figure 22. XRF spectrum fast fitting with interested elements

6.2. Elemental distribution images

The elemental images highlight the chromatic complexity of the painting and the accurate research of the artist in the use of the pigments and in their mixture. The objects have been depicted with richness of particulars for reproducing their ornamental features and to confer as much possible their realistic aspect to the observer. The pigments have been combined for giving the light and shadow effects, the colour brilliance and a three-dimensional vision of the objects by means a meticulous creative process. Further, some colour shades that appear close optically reveal a different chemical nature underlining the artistic choices of the painter in the creative development of the artwork. To analyze given data 5.6.3 version of PyMca software was used by downloading from official website of it. The main elemental images that characterized the artist palette are following reported.

In order to the painting from analyzed point of view was divided as field, ground and center (cows and farmer) part. The main elemental images that characterized the artist palette are following reported comprehensively. As shown in Fig.22 ROI area of spectrum is consist of main elements which are important to predict compositions of used pigments.

White painted layer

Zinc is present throughout the painting and the canvas structure is visible in the zinc distribution map, implying that the zinc rich pigment, no doubt zinc white, must be present in the ground or imprimatura layer.

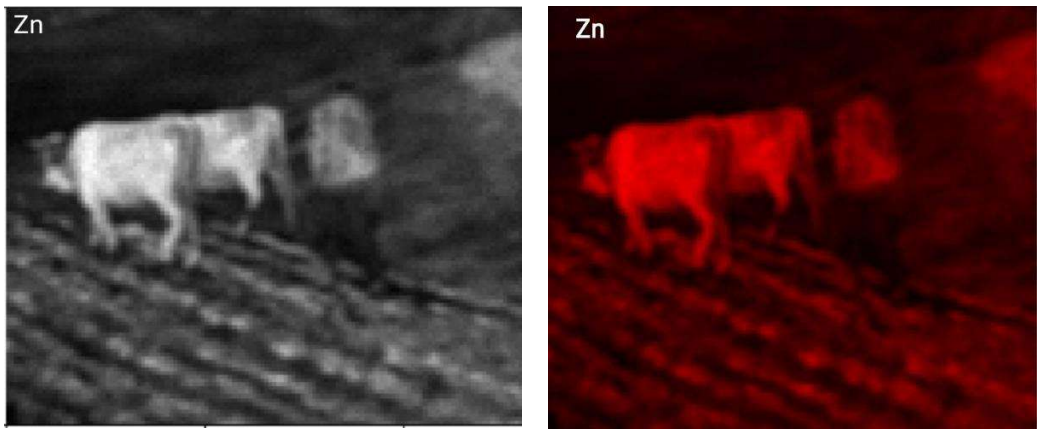

Figure 23. Zn elemental distribution map under grayscale and colorful scale

The main pigments in a paint layer are commonly present at a concentration level of several mass percent. With the scientific progress achieved in the 19th century a number of new pigments were developed. Zinc white (ZnO) was used from the 19th century (Alfeld, Matthias, and José AC Broekaert. 2013).

As it seems clearly from zinc distribution map, painting is intense with Zn specially drawing of cows and farmer clothes. Mostly, using white pigment lead white, barium white, chalk white were widespread, also zinc white were popular pigment in oil paintings. The center part of this painting is not strongly absorbing as it mostly consists of gypsum($CaSO_4 \cdot 2H_2O$) and organic binders thus, while elements lighter than Zn (with characteristic energy lower than 8.6 keV) are only weakly detectable. Mainly, as a Zn white, ZnO(zinc oxide) was using in historical paintings by painters, the center consist of layer of pure zinc white (ZnO) composition was assumed.

Green painted layer

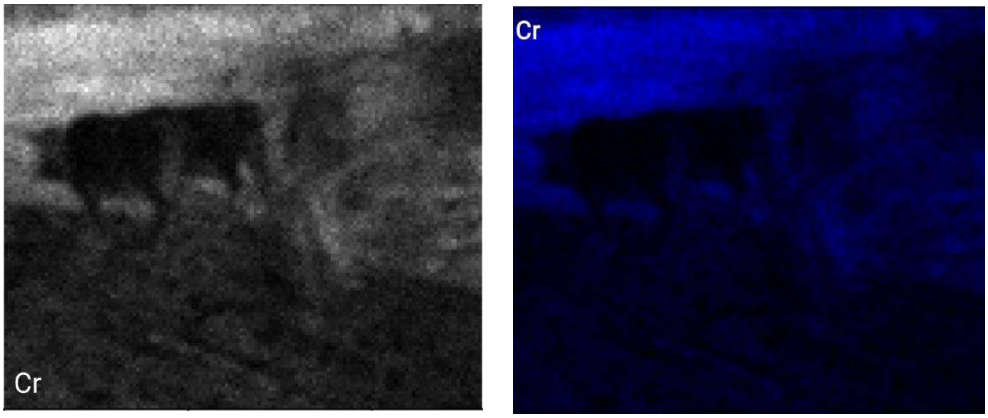

Figure 24. Cr distribution image under grayscale and colorful scale

The most used green inorganic pigments in painted works of art were copper- and chromium-based compounds. There is some confusion about the introduction of chromium(III) oxide under the name "chrome oxide green" and chromium(III) oxide dihydrate ($Cr_2O_3 \cdot 2H_2O$) known as "viridian" for preparation of paints. Although it has been reported the beginning of its use falls in the middle of the 19th century, there is evidence of its use for painting walls in ancient Chinese culture, dating back to 500 BC.

Evidence has also been found in some other works of art from the Roman and Ottoman period (Kahrovic, Emira, Vanja Jakovljevic, and Adnan Zahirovic. 2020) As it seems from Figure 23. in large part of painting Cr was used which covers field area of painting. Due to the color it was assumed that as a green colour chromium(III) oxide was preferred.

Brown painted layer

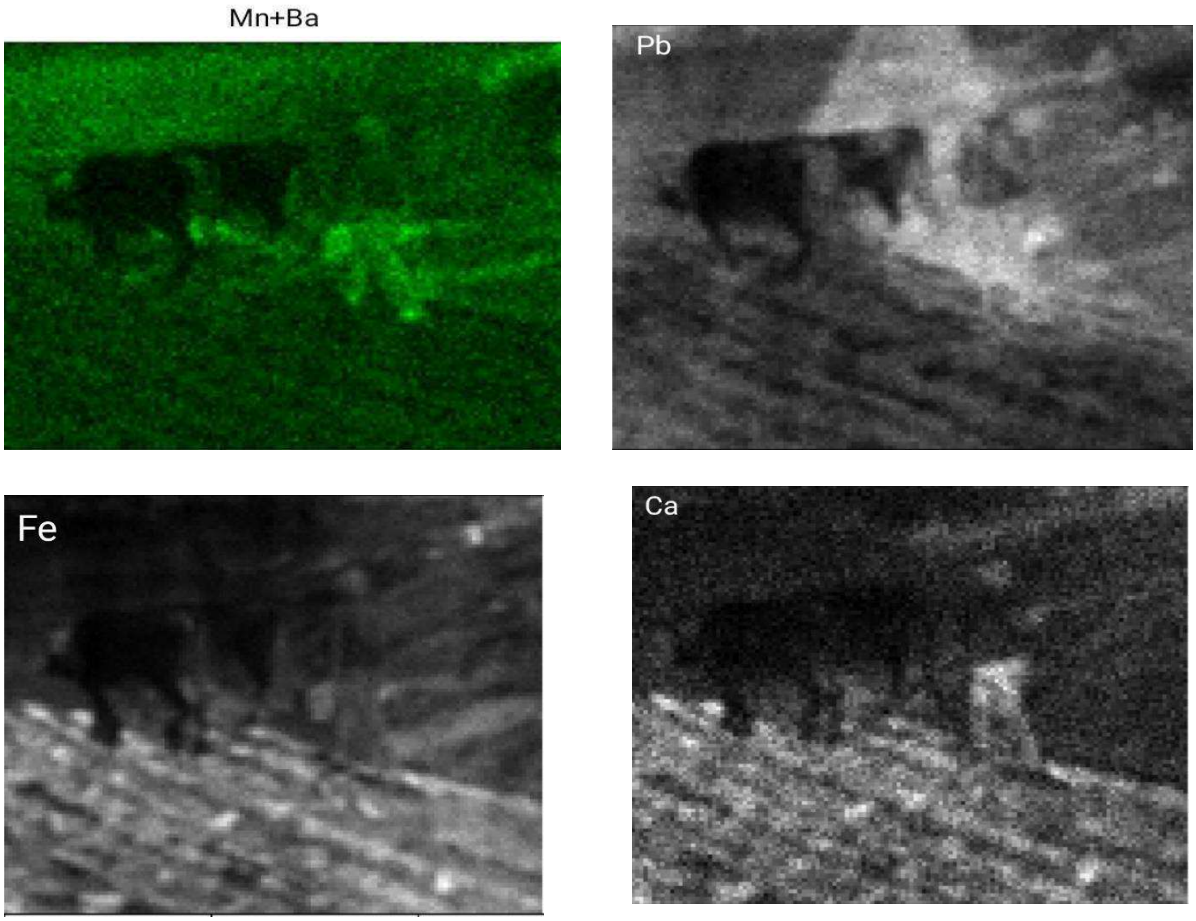

Figure 25. Fe,Mn,Ba,Ca and Pb elemental distribution map

As it seems from Figure 24. ground or soil part of painting was drawn with brown color. Natural brown pigments known under the name burnt amber or simply umber since the 16th century mostly contain MnO_2 and Fe_2O_3 in different proportions, sometimes also congaing clay. Brown layer contains a mixture of hydrated Fe_2O_3 and MnO_2, filers $BaSO_4$ and chalk, and a trace of linseed oil as a binder. Ocher, known as earth pigment or hematite, is a natural pigment that can appear in yellow, red,

orange, and brown shades. The color of ocher can also be affected by the content of other minerals, very often the clay and manganese oxide minerals that give the ocher a dark color (Kahrovic, Emira, Vanja Jakovljevic, and Adnan Zahirovic. 2020). Due to this fact ground layer of painting assumed earth pigments were used for brownish color. Umber could be utilized to get this color which contains iron oxide (Fe_2O_3)and manganese oxide (MnO_2). In figure 24. there was shown Pb distribution map mostly Pb is using as a white pigment (PbO_2), in here it was used to cover general area of painting to give transparence appearance.

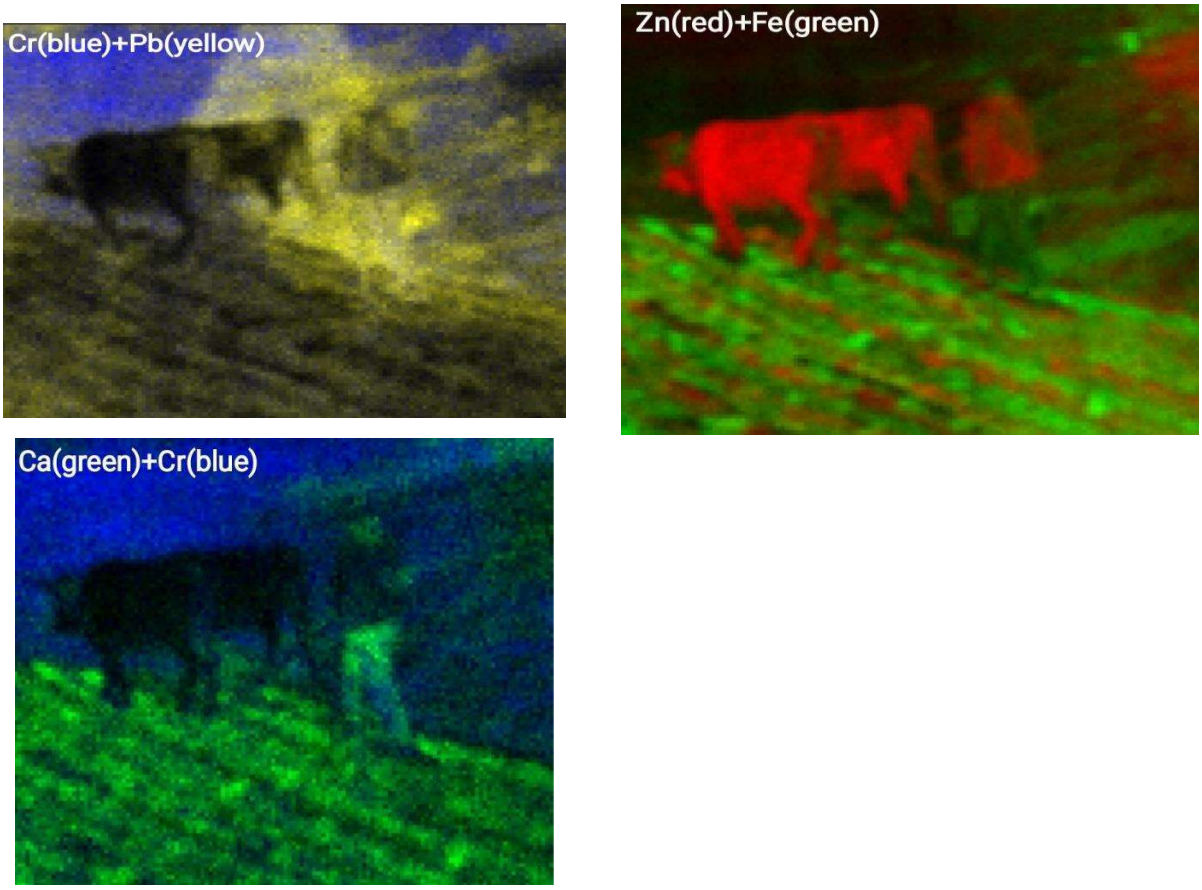

Figure 26. Merge of elemental distribution map under RGB mode

Chapter 7. Conclusion

Paintings are complex multi-layered materials that have been studied over the time with several sophisticated imaging techniques. It is well recognized that analytical result contributed efficaciously to art-history and conservation science.

Scanning MA-XRF technique provides information on pigment materials and their distribution over the painted surface in a non-destructive way, giving new insights on painting techniques used in the various artistic movements over the time. In addition, it provides information on conservation state of artworks allowing to identify appropriate conservation procedures and to identify restoration treatments occurred in the past. MA-XRF is also suitable for approaching question of authenticity of artworks through the presence of anachronistic pigments. Finally, the penetrating nature of X-rays allows visualizing subsurface layers that can present hidden pictorial compositions, revealing what is not visible to naked eye.

A further distinctive feature of the instrument consisted in the development of real-time elaboration procedure of X-ray data. The real-time spectra elaboration offers the advantage to have the available images when the acquisition finish, obtaining a significant gain in terms of time, an immediate preliminary interpretation of data and also the monitoring of a correct progress of the scan. Each pixel spectrum is processed by applying the PyMca fast-fitting plugin based on the non-linear least-squares (NLLS) method. Its integration into the analysis procedure differs from the conventional real-time analysis (if present) of other devices, based on the less accurate selection of region of interest (ROI) in the spectra. The in-house programmed analysis software runs during scan and allows the (near) real-time data transferring with a maximum processing speed up to 5000 fitted spectra per second. In addition, the analysis software provides different tools for processing the images in live mode, by changing graphical settings as color-maps, contrast and brightness, resizing, etc. Arithmetic and logical operations can be also applied to the images for subtracting noise or contaminations and also eventual systematic shift correction can be operated. It allows also the RGB correlation of the maps for helping the pigments identification. Finally, the pixel size of images can be changed during the continuous scanning if images are not satisfactory in terms of lateral resolution or counts statistic.

A MA-XRF investigation of the “Il Contadino” (oil painting on canvas, 35x37 cm) was carried out in collaboration with the private company Ars Mensurae. This allowed to

characterize the original materials used by the artist, highlighting the chromatic complexity of the painting technique and the meticulous research in the use of the pigments and in their mixture. Further, it was possible to identify the some pigments as white, brown, green pigments. By using elemental distribution of map it was predicted that as a white pigment ZnO, brown color earth pigments, as a green color Chromium oxide (Cr_2O_3), additionally, as a background white lead (PbO) had been used. As mentioned before painting are complex and heterogeny materials that is why using one method is not enough to identify actual pigments structure. To get more specific and accurate results additional analysis techniques should be implemented.

Bibliography

1. Abdlaty, Ramy, et al. "Hyperspectral imaging: a comparison of acousto-optic and liquid crystal tunable filters." *Medical Imaging 2018: Physics of Medical Imaging* . Vol. 10573. International Society for Optics and Photonics, 2018.
2. Acquafredda, Pasquale. "XRF technique." *Physical Sciences Reviews* 4.8 (2019).
3. Alfeld, M., and L. De Viguerie. "Recent developments in spectroscopic imaging techniques for historical paintings-a review." *Spectrochimica Acta Part B: Atomic Spectroscopy* 136 (2017): 81-105.
4. Alfeld, Matthias, and José AC Broekaert. "Mobile depth profiling and sub-surface imaging techniques for historical paintings—A review." *Spectrochimica Acta Part B: Atomic Spectroscopy* 88 (2013): 211-230.
5. Alfeld, Matthias, et al. "A mobile instrument for in situ scanning macro-XRF investigation of historical paintings." *Journal of Analytical Atomic Spectrometry* 28.5 (2013): 760-767.
6. Alfeld, Matthias, et al. "MA-XRF and hyperspectral reflectance imaging for visualizing traces of antique polychromy on the Frieze of the Siphnian Treasury." *Microchemical Journal* 141 (2018): 395-403.
7. Alfeld, Matthias, et al. "Optimization of mobile scanning macro-XRF systems for the in situ investigation of historical paintings." *Journal of Analytical Atomic Spectrometry* 26.5 (2011): 899-909.
8. Alfeld, Matthias, Kristina Mösl, and Ina Reiche. "Sunset and moonshine: Variable blue and yellow pigments used by Caspar David Friedrich in different creative periods revealed by in situ XRF imaging." *X-Ray Spectrometry* (2020).
9. Alfeld, Matthias, Victor Gonzalez, and Annelies van Loon. "Data intrinsic correction for working distance variations in MA-XRF of historical paintings based on the Ar signal." *X-Ray Spectrometry*.2020
10. Anitha, A., Brasoveanu, A., Duarte, M., Hughes, S., Daubechies, I., Dik, J., ... & Alfeld, M. (2013). Restoration of X-ray fluorescence images of hidden paintings. Signal Processing, 93(3), 592-604.
11. Appolonia, Lorenzo, et al. "Combined use of FORS, XRF and Raman spectroscopy in the study of mural paintings in the Aosta Valley (Italy)." *Analytical and bioanalytical chemistry* 395.7 (2009): 2005-2013.

12. Artioli, Gilberto, and Ivana Angelini. *Scientific methods and cultural heritage: an introduction to the application of materials science to archaeometry and conservation science*. Oxford University Press, 2010.
13. Barcellos Lins, Sergio Augusto, et al. "Testing the Accuracy of the Calculation of Gold Leaf Thickness by MC Simulations and MA-XRF Scanning." *Applied Sciences* 10.10 (2020): 3582.
14. Barnett, John R., Sarah Miller, and Emma Pearce. "Color and art: A brief history of pigments." *Optics & Laser Technology* 38.4-6 (2006): 445-453.
15. Bertrand, Loïc, et al. "Cultural heritage and archeology materials studied by synchrotron spectroscopy and imaging." *Applied Physics A* 106.2 (2012): 377-396.
16. Brouwer, Peter. "Theory of XRF." *Almelo, Netherlands: PANalytical BV* (2006).
17. Caliri, Claudia. "A mobile xrf scanner for a real-time elemental imaging of painted artworks." (2017).
18. Carlsson, Carl A., and Gudrun Alm Alm Carlsson. *Basic physics of X-ray imaging*. Linköping University Electronic Press, 1973.
19. Cesareo, Roberto. "Portable energy-dispersive X-ray fluorescence equipment for the analysis of cultural heritage." *Pramana* 76.2 (2011): 313-319.
20. Chen, Jiuan Jiuan, Aaron Shugar, and Ashley Jehle. "X - radiography of cultural heritage materials using handheld XRF spectrometers." *X - Ray Spectrometry* 48.4 (2019): 311-318.
21. Clark, Robin JH. "Pigment identification by spectroscopic means: an arts / science interface." *Comptes Rendus Chimie* 5.1 (2002): 7-20.
22. Codling, K., Gudat, W., Koch, E. E., Kotani, A., Lynch, D. W., Rowe, E. M., ... & Toyozawa, Y. (2013). Synchrotron radiation: techniques and applications (Vol. 10). C. Kunz (Ed.). Springer Science & Business Media.
23. Cosentino, Antonino. "Practical notes on ultraviolet technical photography for art examination." *Conservar Património* 21 (2015): 53-62.
24. Creagh, DC, and DA Bradley. "X-ray fluorescence applications for the study and conservation of cultural heritage." *Radiation in Art and Archeometry* (2000): 285.
25. Creagh, Dudley Cecil, and David Bradley. *Physical techniques in the study of art, archeology and cultural heritage* . Elsevier, 2007.
26. dos Santos, Hellen Cristine, et al. "Real-time MA-XRF imaging spectroscopy of the Virgin with the Child painted by Antonello de Saliba in 1497." *Microchemical Journal* 140 (2018): 96-104.

27. Forrest, Craig. *International law and the protection of cultural heritage* . Routledge, 2010.
28. Gibson, David, and Walter Gibson."Polycapillary optics: an enabling technology for new applications." *Advances in X-ray Analysis* 45 (2002): 286-297
29. Gogineni, Rajesh, and Ashvini Chaturvedi. "Hyperspectral Image Classification." *Processing and Analysis of Hyperspectral Data* . IntechOpen, 2019.
30. Goltz, Douglas, et al. "Assessing stains on historical documents using hyperspectral imaging." *Journal of Cultural Heritage* 11.1 (2010): 19-26.
31. Guerra, M., et al. "Performance of three different Si X-ray detectors for portable XRF spectrometers in cultural heritage applications." *Journal of Instrumentation* 7.10 (2012): C10004.
32. Guthrie, James M., and Jeffrey R. Ferguson. "Overview of X-ray Fluorescence." *Archaeometry Laboratory at the University of Missouri Research Reactor. http: // archaeometry. Missouri. edu / xrf_overview. html* (2012).
33. Hain, Miraslov, Jn Bartl, and Viado Jacko. "Multispectral analysis of cultural heritage artefacts." *Measurement Science Review* 3.3 (2003): 9-12.
34. Hocquet, F - P., Et al. "A remote controlled XRF system for field analysis of cultural heritage objects." *X - Ray Spectrometry: An International Journal* 37.4 (2008): 304-308.
35. https://www.exvil.lt/wp-content/uploads/2012/04/SDD_Explained.pdf , Oxfrod instruments
36. Huang, Xiang, et al. "Computational imaging for cultural heritage: Recent developments in spectral imaging, 3-D surface measurement, image relighting, and X-ray mapping." *IEEE Signal Processing Magazine* 33.5 (2016): 130-138.
37. Jackson, J. Bianca, et al. "A survey of terahertz applications in cultural heritage conservation science." *IEEE Transactions on Terahertz Science and Technology* 1.1 (2011): 220-231.
38. Janssens, Koen, et al. "Non-invasive and non-destructive examination of artistic pigments, paints, and paintings by means of X-ray methods." *Analytical Chemistry for Cultural Heritage* . Springer, Cham, 2017. 77-128.
39. Kahrovic, Emira, Vanja Jakovljevic, and Adnan Zahirovic. "FTIR INVESTIGATION OF PIGMENTS AND BINDER OF PAINTED WALLS IN HERITAGE MONUMENTS." *Journal of Science and Arts* 20.3 (2020): 697-704.

40. Kamruzzaman, M., and DW. Hedgehog. "Introduction to hyperspectral imaging technology." *Computer vision technology for food quality evaluation* . Academic Press, 2016. 111-139.
41. Kanngießer, B., N. Langhoff, and R. Wedell. "Handbook of practical X-Ray fluorescence analysis." *Beckhoff, B., Kanngiesser, B., Langhoff, N., Wedell, R., Wolff, H., Eds* (2006): 433-474.
42. Khan, Muhammad Jaleed, et al. "Modern trends in hyperspectral image analysis: a review." *IEEE Access* 6 (2018): 14118-14129.
43. Klein, Marvin E., et al. "Quantitative hyperspectral reflectance imaging." *Sensors* 8.9 (2008): 5576-5618.
44. Knoll, Glenn F. *Radiation detection and measurement* . John Wiley & Sons, 2010.
45. Laclavetine, Kilian, et al. "Macro X-ray fluorescence scanning, multi-and hyperspectral imaging study of multiple layers of paintings on paneled vault in the church of Le Quillio (France)." *X-Ray Spectrometry* (2020).
46. Legrand, Stijn, et al. "Examination of historical paintings by state-of-the-art hyperspectral imaging methods: from scanning infra-red spectroscopy to computed X-ray laminography." *Heritage Science* 2.1 (2014): 13.
47. Liang, Haida. "Advances in multispectral and hyperspectral imaging for archeology and art conservation." *Applied Physics A* 106.2 (2012): 309-323.
48. Lifshin, Eric, ed. *X-ray Characterization of Materials* . John Wiley & Sons, 2008.
49. Lins, Sergio Augusto & Gigante, Giovanni & Cesareo, R. & Ridolfi, Stefano. (2019). Recent developments on portable XRF scanner.
50. Lins, Sergio Augusto Barcellos. *Multispectral analysis of Nuragic metallic samples (Sardinia, Italy)* . MS thesis. Universidade de Évora, 2018.
51. Liritzis, Ioannis, and Nikolaos Zacharias. "Portable XRF of Archaeological Artifacts: Current Research, Potentials and Limitations." *X-ray fluorescence spectrometry (XRF) in geoarchaeology* . Springer, New York, NY, 2011. 109-142.
52. Longoni, A., et al. "A portable XRF spectrometer for non-destructive analyses in archaeometry." *Nuclear instruments and methods in Physics research Section A: Accelerators, spectrometers, detectors and associated equipment* 409.1-3 (1998): 407-409.
53. Margui, Eva, and Rene Van Grieken. *X-ray fluorescence spectrometry and related techniques: an introduction* . Momentum press, 2013.

54. Moropoulou, Antonia, et al. "Multispectral applications of infrared thermography in the diagnosis and protection of built cultural heritage." *Applied Sciences* 8.2 (2018): 284.
55. Neelmeijer, C., et al. "Paintings—a challenge for XRF and PIXE analysis." *X-Ray Spectrometry: An International Journal* 29.1 (2000): 101-110.
56. Padoan, R., et al. "Quantitative hyperspectral imaging of historical documents: technique and applications." *Art Proceedings* (2008): 25-30.
57. Paoletti, ME, et al. "Deep learning classifiers for hyperspectral imaging: A review." *ISPRS Journal of Photogrammetry and Remote Sensing* 158 (2019): 279-317.
58. Pereira, Marcelo & Felix, Valter & Oliveira, Ana & Ferreira, Douglas & Pimenta, André & Carvalho, Cristiano & Silva, Fabricio & Pérez, Carlos & Galante, Douglas & Freitas, Renato. (2020). Investigating counterfeiting of an artwork by XRF, SEM-EDS, FTIR and synchrotron radiation induced MA-XRF at LNLS-BRAZIL. Spectrochimica acta. Part A, Molecular and biomolecular spectroscopy. 246. 118925. 10.1016/j.saa.2020.118925.
59. Picollo, Marcello, et al. "Hyper-Spectral Imaging Technique in the Cultural Heritage Field: New Possible Scenarios." *Sensors* 20.10 (2020): 2843.
60. Pouyet, Emeline, et al. "Development of a highly mobile and versatile large MA-XRF scanner for in situ analyses of painted work of arts." *X-Ray Spectrometry* (2020).
61. Rampazzi, Laura, et al. "Non-invasive techniques for revealing the palette of the Romantic painter Francesco Hayez." *Spectrochimica Acta Part A: Molecular and Biomolecular Spectroscopy* 176 (2017): 142-154.
62. Ravaud, E., et al. "Development of a versatile XRF scanner for the elemental imaging of paintworks." *Applied Physics A* 122.1 (2016): 17.
63. Ricciardi, Paola, et al. "Macro X-ray fluorescence (MA-XRF) scanning of illuminated manuscript fragments: potentialities and challenges." *Microchemical Journal* 124 (2016): 785-791.)
64. Ridolfi, S. "Portable EDXRF in a multi-technique approach for the analyses of paintings." *Insight-Non-Destructive Testing and Condition Monitoring* 59.5 (2017): 273-275.
65. Romani, M., et al. "Analytical chemistry approach in cultural heritage: the case of Vincenzo Pasqualoni's wall paintings in S. Nicola in Carcere (Rome)." *Microchemical Journal* (2020): 104920.

66. Romano, Francesco Paolo, et al. "Real-time elemental imaging of large dimension paintings with a novel mobile macro X-ray fluorescence (MA-XRF) scanning technique." *Journal of Analytical Atomic Spectrometry* 32.4 (2017): 773-781.
67. Rosi, Francesca, et al. "A non-invasive XRF study supported by multivariate statistical analysis and reflectance FTIR to assess the composition of modern painting materials." *Spectrochimica Acta Part A: Molecular and Biomolecular Spectroscopy* 71.5 (2009): 1655-1662.
68. Saverwyns, Steven, Christina Currie, and Eduardo Lamas-Delgado. "Macro X-ray fluorescence scanning (MA-XRF) as a tool in the authentication of paintings." *Microchemical Journal* 137 (2018): 139-147.
69. Saverwyns, Steven, Christina Currie, and Eduardo Lamas-Delgado. "Macro X-ray fluorescence scanning (MA-XRF) as a tool in the authentication of paintings." *Microchemical Journal* 137 (2018): 139-147.
70. Schoonjans, Tom, et al. "The xraylib library for X-ray – matter interactions. Recent developments." *Spectrochimica Acta Part B: Atomic Spectroscopy* 66.11-12 (2011): 776-784.
71. Strüder, L., P. Lechner, and P. Leutenegger. "Silicon drift detector – the key to new experiments." *The Science of Nature* 85.11 (1998): 539-543.
72. Thurrowgood, David, et al. "A hidden portrait by Edgar Degas." *Scientific reports* 6.1 (2016): 1-10.
73. Van der Snickt, Geert, et al. "In situ macro X-ray fluorescence (MA-XRF) scanning as a non-invasive tool to probe for subsurface modifications in paintings by PP Rubens." *Microchemical Journal* 138 (2018): 238-245.
74. Van Espen, P., H. Nullens, and F. Adams. "A method for the accurate description of the full-energy peaks in non-linear least-squares analysis of the X-ray spectra." *Nuclear Instruments and Methods* 145.3 (1977): 579-582.
75. Van Grieken, Rene, and Andrzej Markowicz, eds. *Handbook of X-ray Spectrometry*. CRC press, 2001.